The *C. elegans* TspanC8 tetraspanin TSP-14 exhibits isoform-specific localization and function

Zhiyu Liu, Herong Shi* and Jun Liu**

Department of Molecular Biology and Genetics, Cornell University, Ithaca, NY 14853

* **Deceased**

Corresponding author: Jun Liu, Department of Molecular Biology and Genetics, Cornell University, 439 Biotechnology Building, Ithaca, NY 14853. Tel: 607-254-8942. Fax: 607-255-6249. E-mail: JL53@cornell.edu

Running title: TSP-14 isoform specific function and localization

Key words: tetraspanin; TSP-14; TSP-14A, TSP-14B, TSpanC8; TSP-12, endosome, BMP; TGFβ, apical, basolateral

Author contributions: Z.L., H.S. and J.L. performed experiments, Z.L. and J.L. designed research and wrote the paper.

Abstract

Tetraspanin proteins are a unique family of highly conserved four-pass transmembrane proteins in metazoans. While much is known about their biochemical properties, the in vivo functions and distribution patterns of different tetraspanin proteins are less understood. Previous studies have shown that two paralogous tetraspanins that belong to the TspanC8 subfamily, TSP-12 and TSP-14, function redundantly to promote both Notch signaling and bone morphogenetic protein (BMP) signaling in *C. elegans.* TSP-14 has two isoforms, TSP-14A and TSP-14B, where TSP-14B has an additional 24 amino acids at its N-terminus compared to TSP-14A. By generating isoform specific knock-ins and knock-outs using CRISPR, we found that TSP-14A and TSP-14B share distinct as well as overlapping expression patterns and functions. While TSP-14A functions redundantly with TSP-12 to regulate body size and embryonic and vulva development, TSP-14B primarily functions redundantly with TSP-12 to regulate postembryonic mesoderm development. Importantly, TSP-14A and TSP-14B exhibit distinct subcellular localization patterns. TSP-14A is localized apically and on early and late endosomes. TSP-14B is localized to the basolateral cell membrane. We further identified a di-leucine motif within the N-terminal 24 amino acids of TSP-14B that serves as a basolateral membrane targeting sequence, and showed that the basolateral membrane localization of TSP-14B is important for its function. Our work highlights the diverse and intricate functions of TspanC8 tetraspanins in *C. elegans*, and demonstrates the importance of dissecting the functions of these important proteins in an intact living organism.

45 **Author summary**

46

47 Tetraspanin proteins are a unique family of highly conserved four-pass transmembrane proteins
48 in higher eukaryotes. Abnormal expression of certain tetraspanins is associated with various
49 types of diseases, including cancer. Understanding the functions of different tetraspanin proteins
50 in vivo is crucial in deciphering the link between tetraspanins and their associated disease states.
51 We have previously identified two tetraspanins, TSP-12 and TSP-14, that share redundant
52 functions in regulating multiple aspects of *C. elegans* development. Here we show that TSP-14
53 has two protein isoforms. Using CRISPR knock-in and knock-out technology, we have found
54 that the two isoforms share unique, as well as overlapping expression patterns and functions.
55 Furthermore, they exhibit distinct subcellular localization patterns. Our work highlights the
56 diverse and intricate functions of tetraspanin proteins in a living multicellular organism, and
57 demonstrates that protein isoforms are another mechanism *C. elegans* uses to increase the
58 diversity and versatility of its proteome.

59

60

61 **Introduction**

62 Tetraspanin proteins are a unique family of four-pass transmembrane proteins that are
63 highly conserved in metazoans [1, 2]. There are 33 tetraspanins in humans, 37 in *Drosophila* and
64 21 in *C. elegans*. All tetraspanin proteins contain four transmembrane domains and two
65 extracellular (EC) loops, including the small EC1 loop and the large EC2 loop. The large EC2
66 loop contains a conserved Cys-Cys-Gly (CCG) motif and additional cysteine residues that
67 mediate disulfide bond formation. Based on the number of cysteine residues in the EC2 loop,
68 tetraspanins can be classified into distinct subfamilies. One of them is the TspanC8 subfamily.
69 There are six members of TspanC8 tetraspanins in mammals, Tspan5, Tspan10, Tspan14.
70 Tspan15, Tspan17 and Tspan33 [3, 4]. TspanC8 tetraspanins are known to bind directly to
71 ADAM10 (A Disintegrin and Metalloprotease 10) to regulate its trafficking and function [5-7].
72 Evidence from recent studies showed that different TspanC8s localize ADAM10 to different
73 subcellular compartments and differentially affect the ability of ADAM10 to cleave distinct
74 substrates [8-12]. However, the large number of TspanC8 proteins in mammals makes it
75 technically challenging to comprehensively decipher the endogenous localization and functions
76 of each of these TspanC8 tetraspanins in live animals during development.

77 With the availability of molecular genetic tools to manipulate its genome and the
78 possibility to perform high resolution imaging on live animals, *C. elegans* provides a unique
79 model system for dissectting the functions of TspanC8 tetraspanin proteins in vivo. Unlike
80 mammals, *C. elegans* has only one TspanC8 tetraspanin, TSP-14, which has a paralog TSP-12.
81 Despite being a C6 tetraspanin, TSP-12 functions redundantly with TSP-14 to promote both
82 Notch signaling and BMP signaling [13-15]. Specifically, while animals lacking either TSP-12
83 or TSP-14 do not exhibit any overt phenotypes, animals lacking both TSP-12 and TSP-14 are

84 small (Sma), vulvaless (Vul), exhibit maternal effect embryonic lethality (EMB), and have
85 suppression of the *sma-9(0)* coelomocyte defects (Susm) [16]. The Sma and Susm phenotypes of
86 *tsp-12(0); tsp-14(0)* double mutants are due to defects in BMP signaling, a pathway known to
87 regulate body size and postembryonic mesoderm development in *C. elegans* [17]. We have
88 previously shown that endogenous TSP-12 and TSP-14 are both localized to the plasma
89 membrane and to various intracellular vesicles that include early, late and recycling endosomes
90 [16]. In the early embryo, TSP-12 is required for the cell surface localization of the *C. elegans*
91 ADAM10 ortholog SUP-17 [15]. In hypodermal and intestinal cells in the developing larvae,
92 TSP-12 and TSP-14 function redundantly to regulate the recycling of the type II BMP receptor
93 DAF-4 to the cell surface [16].

94 During the course of these studies, we noticed that the *tsp-14* locus encodes two major
95 protein isoforms, TSP-14A and TSP-14B, that differ by only 24 amino acids at the N-termini.
96 Using a combination of CRISPR knock-in/knock-out technology and high-resolution
97 microscopy, we assessed the endogenous expression, localization, and function of the two
98 different TSP-14 isoforms in live animals. We show here that TSP-14A and TSP-14B share
99 unique and overlapping functions in *C. elegans* development. Moreover, while TSP-14A is
100 localized to apical, intracellular vesicles, TSP-14B is localized to the plasma membrane on the
101 basolateral side. We further identified the basolateral membrane localization signal within the 24
102 amino acids unique to TSP-14B, and showed that this sequence is essential for both the
103 localization and function of TSP-14B. Our work highlights the diverse and intricate functions of
104 TspanC8 tetraspanins in an intact living organism.
105

106 **Results**

107 **The *tsp-14* locus produces two protein isoforms, TSP-14A and TSP-14B, which differ by 24**
108 **amino acids at their N-termini**

109 Sequencing data from existing cDNA clones showed that the *tsp-14* locus produces two
110 major TSP-14 isoforms, *tsp-14a* and *tsp-14b*, which share the same 3' ends, but differ at their 5'
111 ends (wormbase.org). Specifically, *tsp-14b* uses an upstream alternative 35bp first exon. While
112 the second exon of *tsp-14b* and the first exon of *tsp-14a* share the same 3' ends, *tsp-14b* has an
113 additional 163bp segment upstream of the shared 126bp sequences (Figure 1A). Thus the *tsp-14*
114 locus is predicted to produce two protein isoforms, TSP-14A and TSP-14B, which differ at their
115 N-termini, with TSP-14B having an extra 24 amino acids at its N-terminus compared to TSP-
116 14A (Figure 1B-1C). Both isoforms share the same four transmembrane domains, two
117 extracellular loops that include eight conserved cysteine residues in the second extracellular
118 loop, and an intracellular C-terminal tail. Whether there is any functional significance regarding
119 the presence of the two TSP-14 isoforms was not yet known.
120

121 **TSP-14A and TSP-14B have distinct and shared functions during *C. elegans* development**

122 To determine the functional significance of the two TSP-14 isoforms, we used
123 CRISPR/Cas9 to generate isoform specific knock-outs, *tsp-14a(0)* and *tsp-14b(0)* (Figure 2A,
124 Supplemental Figure 1A). Because the start codon of TSP-14A also encodes a methionine
125 residue in TSP-14B, we mutated it from methionine (ATG) to isoleucine (ATA) to generate the
126 *tsp-14a* null allele *jj304(tsp-14a(0)*). We reasoned that this methionine to isoleucine change can
127 prevent the translation of TSP-14A without significant disruption of the TSP-14B coding
128 sequence (Figure 2A, Supplemental Figure 1A). To generate the *tsp-14b* null allele *jj317(tsp-*
129 *14b(0))*, we mutated the ATG start codon of TSP-14B and a downstream in-frame ATG codon to

130 TTG and TTA respectively (Figure 2A, Supplemental Figure 1A). Because *tsp-14* null mutants
131 have no phenotype on their own, but display multiple phenotypes in the *tsp-12(0)* background
132 due to the functional redundancy shared by *tsp-14* and *tsp-12* [13, 15], we tested the functionality
133 of *tsp-14a(0)* and *tsp-14b(0)* by introducing each allele into the *tsp-12* null background. For this
134 purpose, we used a known deletion allele of *tsp-12*, *ok239*, as well as a new deletion allele *jj300*
135 that we generated via CRISPR (Supplemental Figure 1B). Both alleles will be denoted as *tsp-*
136 *12(0),* unless specified. As shown in Figure 2, *tsp-12(0); tsp-14(0)* double null mutants are small
137 (Sma), vulvaless (Vul), and exhibit 100% maternal effect embryonic lethality (EMB) and a high
138 penetrance (80%) of suppression of the *sma-9(0)* coelomocyte defects (Susm) ([16], Figure 2B,
139 2F-H, 2P). Like *tsp-12(0); tsp-14(0)* double null mutants, *tsp-12(0); tsp-14a(0)* mutants are also
140 Sma, Vul, and 100% EMB (Figure 2B, 2I-K). But *tsp-12(0); tsp-14a(0)* mutants only exhibit a
141 19.4% penetrance of the Susm phenotype (Figure 2P), a very slight increase of penetrance than
142 that of *tsp-12(0)* single null mutants (16.5%). Conversely, *tsp-12(0); tsp-14b(0)* mutants have a
143 normal body size, do not exhibit any vulva defects or embryonic lethality, yet exhibit a 37%
144 penetrance of the Susm phenotype (Figure 2B, 2L-N, 2P). These results suggest that TSP-14A
145 and TSP-14B have distinct functions during *C. elegans* development: TSP-14A shares redundant
146 functions with TSP-12 in regulating body size, embryonic and vulva development, while TSP-
147 14B functions redundantly with TSP-12 in regulating postembryonic mesoderm development.
148 Because *tsp-12(0); tsp-14(0)* double null mutants exhibit a 80% penetrance of the Susm
149 phenotype, higher than that of either *tsp-12(0); tsp-14a(0)* or *tsp-12(0); tsp-14b(0)* mutants
150 (Figure 2P), TSP-14A and TSP-14B must share redundant functions with each other, and with
151 TSP-12, in regulating postembryonic mesoderm development.
152

153 **Single-copy transgene analysis supports distinct and overlapping functions of TSP-14A and**
154 **TSP-14B**

155 One caveat with the CRISPR-mediated knock-out experiments is that certain editing
156 manipulations of one isoform could unavoidably affect the other one. To overcome this problem,
157 we expressed TSP-14A or TSP-14B as single copy transgenes into the same neutral genomic
158 environment [18], which allows for direct comparison of the functionality of the two isoforms.
159 We chose the *ttTi4348* locus on Chromosome I as the insertion site and examined the function of
160 each isoform on its own in the *tsp-12(0); tsp-14(0)* double null background. We used two
161 different *tsp-14* promoter elements to drive the expression of cDNAs encoding either TSP-14A
162 or TSP-14B: a 3.3kb promoter element, which is immediately upstream of the ATG of TSP-14A,
163 and a 5.2kb promoter element, which includes another 1.9kb sequence upstream of the ATG of
164 TSP-14B (Supplemental Figure 2, see also materials and methods). Both promoter elements can
165 drive GFP reporter expression in multiple cell types, including hypodermal cells (hyp 7 and seam
166 cells), although we detected stronger and less mosaic reporter expression under the 5.2kb
167 promoter (Supplemental Figure 2B, 2C). Using both the 3.3kb and the 5.2kb promoter elements
168 to drive the expression of *tsp-14* as single copy transgenes, TSP-14A failed to rescue, while TSP-
169 14B partially rescued, the Susm phenotype of *tsp-12(0); tsp-14(0)* double mutants (Figure 3A,
170 3B). This is consistent with the notion that TSP-14B plays a major role in postembryonic
171 mesoderm development, but normal postembryonic development requires both TSP-14A and
172 TSP-14B as well as TSP-12. Intriguingly, TSP-14A and TSP-14B each on its own can
173 significantly rescue the body size defects of *tsp-12(0); tsp-14(0)* double mutants, with more
174 efficient rescue observed when expression was driven by the longer 5.2kb *tsp-14* promoter as
175 compared with the 3.3kb promoter (Figure 3C). Taken together, the above results support the

176 notion that TSP-14A and TSP-14B exert distinct and overlapping functions in regulating body
177 size and mesoderm development.
178
179 **Endogenous TSP-14A and TSP-14B exhibit distinct expression and localization patterns**
180 To understand the basis underlying the distinct and shared functions of TSP-14A and
181 TSP-14B, we used CRISPR/Cas9-mediated homologous recombination to tag each of the
182 isoforms and examined their expression and subcellular localization patterns. We used two
183 different approaches to tag each of the isoforms.
184 First, we inserted GFP and three copies of the FLAG tag (3xFLAG) at their respective N-
185 termini after the ATG start codons. This led to the generation of N-terminally tagged TSP-14B
186 (*jj192*) and TSP-14A (*jj183)* (Figure 4A, materials and methods). We verified the successful
187 tagging of each isoform by western blot analysis, which also indicated that TSP-14A is
188 expressed at a much higher level compared to TSP-14B (Figure 4D). As expected, both *jj183* and
189 *jj192* animals are healthy and fertile, although *jj183* worms are slightly longer than wild-type
190 worms at the same developmental stage (Figure 4B). We then introduced *jj183* and *jj192* into the
191 *tsp-12(0)* null background, and examined their phenotypes. *tsp-12(0); tsp-14(jj183)* and *tsp-*
192 *12(0); tsp-14(jj192)* animals are both viable and fertile, without any embryonic lethality (Figure
193 4B-C, Supplemental Figure 3), suggesting that neither tag significantly disrupts TSP-14 function.
194 *tsp-12(0); tsp-14(jj183)* animals have a normal body size (Figure 4B, Supplemental Figure 3A),
195 but exhibit a slight increase in penetrance of the Susm phenotype compared to *tsp-12(0)* single
196 mutants (Figure 4C, Supplemental Figure 3B). Because the first coding exon of TSP-14A is part
197 of the second coding exon of TSP-14B (Figure 4A), we suspect that the slight increase in the
198 penetrance of the Susm phenotype in *tsp-12(0); tsp-14(jj183)* animals is likely due to the GFP

199 tag affecting the proper expression or splicing of TSP-14B. Surprisingly, *tsp-12(0); tsp-14(jj192)*
200 mutants have a significantly lower penetrance of the Susm phenotype compared to that of *tsp-*
201 *12(0)* single mutants (Figure 4C, Supplemental Figure 3B). This improved Susm phenotype may
202 be due to the higher expression level of GFP::3xFLAG::TSP-14B compared to the endogenous
203 level of TSP-14B (Figure 4D, see below).

204 We have previously tagged TSP-14 endogenously at its C-terminus with GFP::3xFLAG
205 (*jj219*, Figure 3A) and showed that *jj219*, which has both TSP-14A and TSP-14B tagged, is fully
206 functional [16]. Therefore, as an alternative approach to specifically tag TSP-14A or TSP-14B,
207 we introduced the same GFP::3xFLAG tag as in *jj219* into either *jj304(tsp-14a(0)*) or *jj317(tsp-*
208 *14b(0))*, and generated *jj304 jj319*, which has C-terminally tagged TSP-14B without any TSP-
209 14A, and *jj317 jj377*, which has C-terminally tagged TSP-14A without any TSP-14B (Figure
210 4A). Both *jj304 jj319* and *jj317 jj377* animals behaved similarly as their respective untagged
211 counterparts, *jj304(tsp-14a(0)*) and *jj317(tsp-14b(0))*. Western blots confirmed the specific
212 tagging of TSP-14 isoforms in *jj304 jj319* and *jj317 jj377* animals (Figure 4D). Notably, *jj192*
213 animals (N-terminally tagged TSP-14B + untagged TSP-14A) appear to have an elevated amount
214 of TSP-14B protein than both *jj304 jj319* animals (C-terminally tagged TSP-14B without
215 endogenous TSP-14A) and *jj219* animals (C-terminally tagged TSP-14A + C-terminally tagged
216 TSP-14B) (Figure 4D). The underlying basis is currently unknown.

217 Using the various strains generated above. we conducted high resolution imaging using
218 the Aryscan imaging system (materials and methods). We found that TSP-14A and TSP-14B
219 exhibit distinct expression and localization patterns. First, only TSP-14A, but not TSP-14B, is
220 detectable in the germline and sperm cells, as well as at the tip of the anterior sensory cilia
221 (Figure 5A, 5B), while TSP-14B is detectable in the pharynx (Figure 5F). Both TSP-14A and

222 TSP-14B are found in hypodermal cells (Figure 5C, 5G, 5K, 5P, 5S, 5V) and the developing
223 vulva (Figure 5E, 5I, 5M, 5O, 5R, 5U). However, the two isoforms exhibit different subcellular
224 localization patterns. In hypodermal cells, TSP-14A is primarily localized in intracellular
225 vesicles, while TSP-14B is mainly localized on the cell surface (compare Figures 5C vs. 5G, and
226 Figures 5S vs. 5V). In the developing vulva, TSP-14A is localized on the apical side, while TSP-
227 14B is localized on the basolateral membrane (compare Figures 5E vs. 5I, and Figures 5R vs.
228 5U, for worms at the L4 Christmas-tree stage). Similar localization patterns hold true in the
229 pharynx (Figures 5A, 5F, 5J). Consistent with the higher levels of TSP-14A protein that we
230 detected on western blots (Figure 4E), the TSP-14A signals are significantly brighter than TSP-
231 14B under the microscope (see Figure 5J, 5K, 5M, 5O when both TSP-14A and TSP-14B are
232 present). Thus, TSP-14A and TSP-14B exhibit distinct expression and localization patterns.
233

234 **TSP-14A is localized to early and late endosomes**

235 We have previously shown that TSP-14 is localized to early, late, and recycling
236 endosomes, that it co-localizes with TSP-12 and shares functional redundancy with TSP-12 in
237 promoting BMP signaling [16]. Because TSP-14A is localized to intracellular vesicles, we
238 further examined its localization relative to various endosomal markers and to TSP-12. As shown
239 in Figure 6, TSP-14A co-localizes with TSP-12 (Figure 6B-6H). Furthermore, TSP-14A co-
240 localizes with both the early endosome marker RAB-5 and the late endosome marker RAB-7, but
241 shows little co-localization with the recycling endosome marker RAB-11 (Figure 6I-6R). Given
242 that we previously detected recycling endosome localization of TSP-14 using *jj219*, which labels
243 both TSP-14A and TSP-14B [16], our findings suggest that the very faint vesicular signal from
244 TSP-14B may come from recycling endosomes. However, due to the very weak signal of TSP-

245 14B and the limited number of TSP-14B-positive vesicles, we have not been able to address this
246 question using the reagents that we generated. Nevertheless, our findings suggest that TSP-14A
247 is localized to different endosomal vesicles.
248

249 **TSP-14B is sufficient on its own to localize to the basolateral membrane of polarized cells**

250 Our finding that TSP-14B::GFP::3xFLAG in *tsp-14a* null *(jj304 jj319*) animals is
251 localized to the basolateral surface of vulval and hypodermal cells (Figure 5R-5T) suggests that
252 the basolateral localization of TSP-14B does not require the presence of TSP-14A. To directly
253 test this hypothesis, we forced the expression of C-terminally-tagged TSP-14B as a single copy
254 transgene (*jjSi395*) in *tsp-14(0)* null background using a heterologous *snx-1* promoter. As a
255 control, we also forced the expression of C-terminally TSP-14A (*jjSi393*) using the same
256 approach. In the *tsp-14(0)* null background, TSP-14B (*jjSi395)* is localized to the basolateral
257 membrane of pharyngeal and intestinal cells, while the TSP-14A (*jjSi393*) signal is only weakly
258 detectable in intracellular vesicles in the intestine (Figure 7A,7B). Thus, in the absence of TSP-
259 14A, TSP-14B alone is sufficient to localize to the basolateral membrane of polarized cells. This
260 result suggests that the basolateral membrane targeting sequence resides in the coding region of
261 TSP-14B.
262

263 **TSP-14B contains a basolateral membrane targeting signal in its first 24 amino acids**

264 Since the only difference between TSP-14A and TSP-14B is the N-terminal 24 amino
265 acids present in TSP-14B, we reasoned that these 24 amino acids may contain signal(s) that
266 targets TSP-14B to the basolateral membrane. Indeed, we found an EQCLL motif (Figure 8A)
267 within these 24 amino acids in TSP-14B, similar to the well characterized di-leucine basolateral

268 targeting sequence [DE]xxxL[LI] [19, 20]. Using the CRISPR/Cas9 system, we mutated the
269 EQCLL sequence into AQCAA in the *jj192*(GFP::3xFLAG::TSP-14B) background (Figure 8B)
270 and obtained *tsp-14(jj322 jj192)* (Figure 8E, Supplemental Figure 1C). We found that the GFP-
271 tagged AQCAA mutant TSP-14B protein in *jj322 jj192* worms becomes localized to the apical
272 side of the developing vulva (compare Figure 8C vs 8F) and in intracellular vesicles of
273 hypodermal cells (Figure 8D vs. 8G), just like TSP-14A. These results demonstrate that TSP-
274 14B's localization to the basolateral membrane depends on the EQCLL motif.

275 To examine the functional consequences of having TSP-14B mis-localized, we
276 introduced the AQCAA mutation into wild-type worms via CRISPR and obtained *tsp-14(jj368)*
277 (Figure 8A, Supplemental Figure 1C). We then introduced *jj368* into the *tsp-12(0)* background
278 and examined the phenotypes of *tsp-12(0); tsp-14(jj368)* double mutants. We found that *tsp-*
279 *12(0); tsp-14(jj368)* double mutants [*tsp-12* null mutants with mis-localized TSP-14B] exhibit
280 more severe EMB, body size and and more penetrant Susm phenotypes compared to *tsp-12(0);*
281 *tsp-14(jj317)* double mutants [*tsp-12* null mutants without any TSP-14B] (compare Figure 8H vs.
282 Figure 2B, and compare Figure 8I vs. Figure 2P). Moreover, *tsp-12(0); tsp-14(jj368)* double
283 mutants exhibit a significantly reduced brood size (Figure 8J) and severe embryonic lethality
284 (77% EMB), phenotypes not displayed by *tsp-12(0); tsp-14(jj317)* double mutants. We reasoned
285 that these phenotypes seen in the *tsp-12(0); tsp-14(jj368)* double mutants cannot simply be due
286 to the mis-localization of TSP-14B. Because the EQCLL motif is located right upstream of the
287 ATG codon of TSP-14A (Figure 8A), mutating this motif may have affected a cis-regulatory
288 element(s) important for the proper expression of TSP-14A. To test this hypothesis, we tagged
289 both TSP-14A and TSP-14B in the *jj368* background at their C-terminal ends using CRISPR,
290 and generated *tsp-14(jj368 jj378*, Figure 8K). As suspected, *tsp-14(jj368 jj378*) worms have very

291 little TSP-14A or TSP-14B protein that is detectable on western blots (Figure 4D) and via
292 imaging (Figure 8L). Any detectable TSP-14 protein in *tsp-14(jj368 jj378*) animals appears to be
293 apical and intracellularly localized (Figure 8L). We noticed that *tsp-14(jj368)* single mutants
294 exhibit a 20% Susm phenotype, while *tsp-14(0)* null mutants do not show any Susm phenotype
295 (Figure 8I), suggesting that mis-targeting TSP-14B to the apical side may have a dominant
296 negative effect on TSP-14 and TSP-12 function.
297

298 **Discussion**

299 Despite extensive biochemical studies of the tetraspanin family of proteins, there are
300 significant gaps in our understanding of how different tetraspanin proteins function in vivo in
301 different cellular and developmental contexts. A major challenge for dissecting the in vivo
302 functions of multi-member families of proteins, such as the tetraspanins, in vertebrates is the
303 functional redundancy shared by different members of the same family or subfamily, or by
304 different isoforms of the same protein (for example, [21, 22]). In this study, we used CRISPR-
305 mediated knock-in and knock-out technology and showed that two isoforms of a single *C.*
306 *elegans* TspanC8 tetraspanin, TSP-14A and TSP-14B, exhibit distinct subcellular localization
307 patterns, and share overlapping as well as unique expression patterns and functions. Our work
308 highlights the diverse and intricate functions of TspanC8 tetraspanins in a living organism. It
309 also adds another example to the existing literature that shows protein isoforms are another way
310 for *C. elegans* to increase the diversity and versatility of its proteome.

311 Our isoform specific knock-in experiments showed that TSP-14B is localized to the
312 basolateral membrane, while TSP-14A is localized to the early and recycling endosomes on the
313 apical side of polarized epithelial cells. We further identified a basolateral membrane targeting

314 sequence (EQCLL) within the N-terminal 24 amino acids unique to TSP-14B, and showed that
315 this ExxLL motif is critical for the basolateral membrane localization of TSP-14B. The ExxLL
316 di-leucine motif in TSP-14B differs slightly from the canonical [DE]xxxL[LI] di-leucine motif,
317 which has been previously found to serve as a basolateral membrane targeting sequence (for
318 reviews, see [19, 20]). Basolateral sorting of proteins with the canonical [DE]xxxL[LI] di-
319 leucine motif is primarily mediated by the AP-2 clathrin adaptor, although it can also be
320 mediated by the AP-1 adaptor (for reviews, see [19, 20]). Both AP-1 and AP-2 adaptor
321 complexes exist in *C. elegans* [23-26]. Future work will determine whether the AP-1 or the AP-2
322 adaptor is involved in sorting TSP-14B to the basolateral membrane.

323 To date, most TspanC8 tetraspanins have been reported to be either cell surface or
324 intracellularly localized in cultured cells, most of which are non-polarized [5, 8, 12, 27]. Our
325 findings suggest that some TspanC8 proteins may also exhibit distinct localization patterns in
326 polarized cells. Indeed, a recent report showed apical junction localization of the TspanC8
327 member Tspan33 in polarized mouse cortical collecting duct (mCCD) cells [9]. In the same
328 study, the authors reported that another TspanC8 protein, Tspan15, is not on the apical plane, but
329 is instead localized along lateral contacts of polarized mCCD cells [9]. Whether other TspanC8
330 tetraspanins or their specific isoforms also exhibit distinct subcellular localization patterns in
331 polarized epithelial cells remains to be determined.

332 How the apically localized TSP-14A and basolateral membrane-localized TSP-14B exert
333 their distinct, as well as overlapping, functions in vivo is currently not well understood.
334 Nevertheless, our studies provide clues for the cellular basis underlying the functional
335 redundancy shared by TSP-12 and TSP-14. TSP-14 is known to function redundantly with its
336 paralog TSP-12 to promote both Notch signaling and BMP signaling [13, 15, 16]. Specifically,

337 *tsp-12(0); tsp-14(0)* double null mutants exhibit maternal-effect embryonic lethality (Emb) and
338 are egg-laying defective (Egl) due to defects in vulva development, two processes known to be
339 regulated by Notch signaling [13]. *tsp-12(0); tsp-14(0)* double null mutants are also small and
340 exhibit a suppression of the *sma-9(0)* postembryonic mesoderm defect (Susm), processes
341 regulated by BMP signaling [17, 28]. Like TSP-14, TSP-12 is localized to various endosomes, as
342 well as on the basolateral membrane of polarized vulval and intestinal epithelial cells [16].
343 Animals lacking TSP-12 and TSP-14A share the same penetrance (100%) of Emb and Egl
344 phenotypes as *tsp-12(0); tsp-14(0)* double null animals, suggesting that endosome-localized
345 TSP-12 and TSP-14A are critical for most, if not all, of the biological processes regulated by
346 Notch signaling. In contrast, BMP-regulated body size and postembryonic mesoderm patterning
347 appear to require both TSP-14A and TSP-14B to function together with TSP-12. Yet the
348 contributions of TSP-14A and TSP-14B towards these two BMP-regulated processes are not
349 equal. Three lines of evidence suggest that TSP-14B, but not TSP-14A, is the major player that
350 functions redundantly with TSP-12 in patterning the postembryonic mesoderm. First, animals
351 lacking TSP-12 and TSP-14B (but not TSP-14A) exhibit a higher penetrance of the Susm
352 phenotype than that of *tsp-12(0)* single mutants (Figure 2). Second, when introduced as a single
353 copy transgene, TSP-14B, but not TSP-14A, could partially rescue the Susm phenotype of *tsp-*
354 *12(0); tsp-14(0)* double null mutants (Figure 3). Third, a moderate increase in the level of TSP-
355 14B in *jj192* animals (GFP::3xFLAG::TSP-14B) was sufficient to partially compensate for the
356 lack of TSP-12 in *tsp-12(0)* null mutants in patterning the postembryonic mesoderm (Figure 4,
357 Figures S3). Consistently, when *tsp-14b* was overexpressed as a transgene in the *tsp-12(0); tsp-*
358 *14(0)* double null background, the penetrance of the Susm phenotype is also lower than that seen
359 in *tsp-12(0)* single mutants (Figures S2). Despite this shared redundancy between TSP-12 and

360 TSP-14B in mesoderm patterning, TSP-14A also plays a role in this process, as the penetrance of
361 the Susm phenotype in *tsp-12(0); tsp-14(0)* double null mutants is higher than that of *tsp-12(0);*
362 *tsp-14b(0)* animals (Figure 2).

363 The roles of TSP-14A and TSP-14B in body size regulation appear more complicated. On
364 the one hand, knockout experiments suggest that TSP-14A plays a major role in regulating body
365 size, as *tsp-12(0); tsp-14a(0)* double mutants have a smaller body size, although they are not as
366 small as the *tsp-12(0); tsp-14(0)* double null mutants (Figure 2). On the other hand, forced
367 expression of either TSP-14A or TSP-14B can partially rescue the small body size phenotype of
368 *tsp-12(0); tsp-14(0)* double null mutants (Figure 3). Furthermore, increased amount of TSP-14B
369 in *tsp-12(0); tsp-14(jj192)* mutants [with endogenous TSP-14A but without TSP-12] led to both
370 a slight decrease in body size and a less penetrant Susm phenotype (Figure 4B, Supplemental
371 Figure 3A), suggesting possible antagonistic roles of TSP-14B in the regulation of body size vs.
372 mesoderm development. These functional differences of TSP-14A and TSP-14B may be due to a
373 combination of their unique expression and localization patterns, and ultimately, to the distinct
374 molecular interactions at their specific cellular and subcellular environment.

375 Tetraspanins can have homotypic and heterotypic interactions to organize membranes
376 into tetraspanin-enriched microdomains, and regulate the trafficking or clustering of different
377 membrane or membrane-associated proteins [2, 29-31]. For example, TspanC8 tetraspanins are
378 known to bind and directly regulate the maturation and cell surface localization of ADAM10 [5-
379 7], which is a metalloprotease that cleaves the Notch receptor in *C. elegans*, Drosophila, and
380 mammals. We have previously shown that the *C. elegans* ADAM10, called SUP-17, is also
381 involved in regulating BMP signaling, and that the neogenin homolog UNC-40 may be one of
382 the SUP-17/ADAM10 substrates in regulating BMP signaling [15]. We further showed that TSP-

383 12, but not TSP-14, is required for the cell surface localization of SUP-17/ADAM10 in the early
384 embryo [15]. In addition, TSP-12 and TSP-14 function redundantly to promote the trafficking
385 and cell surface localization of the BMP type II receptor DAF-4 in the developing larvae [16]. It
386 will be important to determine the specific contributions that TSP-14A and TSP-14B each makes
387 towards these TSP-14-mediated functions, and how each of the isoforms works at the molecular
388 level. Finally, both TSP-12 and TSP-14 are also expressed in tissues beyond the sites where
389 BMP signaling and Notch signaling act. They could in principle regulate the trafficking and/or
390 localization of other proteins in addition to SUP-17/ADAM10 and DAF-4/BMPRII. The
391 identification of additional proteins trafficked by TSP-12 and TSP-14 (either TSP-14A or TSP-
392 14B or both), and subsequent determination on how TSP-12 and TSP-14 regulate their
393 trafficking/localization will elucidate how these two tetraspanin proteins function during the
394 development of a multicellular living organism like *C. elegans*. The information obtained could
395 shed light on the myriad of complex functions of the various TspanC8 proteins in mammals, and
396 ultimately aid in the development of therapeutic strategies for the treatment of various diseases
397 caused by abnormal expression or function of certain tetraspanins [32-34].
398

399 **Materials and Methods**

400 ***C. elegans* strains and molecular reagents**

401 *C. elegans* strains used and generated in this study are listed in Supplemental Table S1.
402 All *C. elegans* strains used in this study are derived from the Bristol N2 strain, maintained at
403 20°C (unless otherwise noted). Oligonucleotides and plasmids used and generated in this study
404 are listed in Supplemental Table S2.
405

406 **Body size measurement and *sma-9(0)* suppression assays**

407 Body size measurement and the *sma-9(0)* suppression assays were performed following
408 the methods described in [35]. Hermaphrodite worms at the L4 Christmas-tree stage (based on
409 the developing vulva) were used for body size measurement. Images of worms were taken using
410 a Leica DMR2 compound microscope equipped with a Hamamatsu Orca-03G camera using the
411 iVision software (BioVision Technologies). The length of each worm was then measured
412 using segmented lines in the open-source software Fiji. Body length of at least 30 worms per
413 genotype were measured. For the *sma-9(0)* coelomocyte suppression (Susm) assays, strains
414 expressing the *CC::gfp* marker *arIs37(secreted CC::gfp)* or *ccIs4438(intrinsic CC::gfp)* in
415 specific mutant backgrounds were generated (Table S1). Hermaphrodite worms with GFP-
416 labeled coelomocytes (CCs) were scored at the young adult stage under a Nikon SMZ1500 stereo
417 zoom microscope equipped with a Sola light engine (Lumencor). For each genotype, two
418 independent isolates were used and worms from three to five plates per isolate were scored. For
419 each plate, the number of worms with 5-6 CCs was divided by the total number of worms
420 examined to determine the penetrance of the Susm phenotype. For statistical analysis, an
421 ANOVA and Tukey's honestly significant difference (HSD) test were performed to test
422 differences in body size and Susm penetrance between different genotypes using R.
423

424 **CRISPR/Cas9 experiments**

425 For all CRISPR/Cas9 experiments, Cas9 target sites were chosen using the CRISPR
426 online design tool CHOPCHOP (http://chopchop.cbu.uib.no). Oligos with the single-guide
427 (sg)RNA sequences used to generate the sgRNA-expressing plasmids (using method described in
428 [36]) are listed in Table S2. For the knockout experiments, two sgRNA targeting sites, one

429 around the start codon, and the other around the stop codon, of the gene, were chosen in order to
430 completely knockout the gene of interest. To generate point mutations using the CRISPR/Cas9
431 system, single stranded DNA oligos (listed in Table S2) were used as the homologous repair
432 templates. To endogenously tag the different TSP-14 isoforms, plasmids containing the
433 homologous repair templates were generated by following the method described by Dickinson et
434 al [37]. Specifically, ~600-bp homology arms for each target locus were amplified from N2
435 genomic DNA and then inserted into the GFP^SEC^3xFlag vector pDD282 or the
436 TagRFP^SEC^3xMyc vector pDD286 via Gibson Assembly (New England BioLabs).
437 Hygromycin was used to select the knock-in candidate lines based on the strategy described in
438 Dickinson et al [37].
439 For the single-copy insertion rescue experiments, we followed the strategy described by
440 Pani and Goldstein [38] and chose *ttTi4348* on chromosome I as the insertion site. pAP082 was
441 the plasmid used for the expression of Cas9 and sgRNA [38]. Repair templates were generated
442 by replacing the ClaI and AvrII fragment in pAP088 with various fragments containing the
443 specific promoter, cDNA or chimeric cDNA-gDNA of the specific gene, and the specific 3'UTR.
444 All plasmids used in CRISPR/Cas9 experiments are listed in Table S2.
445

446 **Live imaging and image analysis**

447 L4 stage or young adult worms were mounted on 2% agarose pads with 10 mM
448 levamisole (CAS 16595-80-5; Sigma-Aldrich). A Zeiss LSM i880 microscope with Airyscan
449 equipped with 40× Fluar objective (N.A. 1.3) or 60× Plan-apochromat objective (N.A. 1.4) using
450 Immersol 518F oil (Carl Zeiss) was used to capture both the fluorescent and differential
451 interference contrast (DIC) images at super-resolution. Images were viewed and processed with

452 ZEN software. GFP was excited at 488 nm, and RFP or TagRFP was excited at 561 nm. GFP
453 emission was captured with the BP495-550 filter, and RFP or TagRFP emission was captured
454 with the LP570 filter. To determine the subcellular localization of GFP::TSP-14A, and the co-
455 localization of TSP-14A with TSP-12, quantitative colocalization analysis was performed using
456 the JACoP plugin of the open-source Fiji software [39]. For each image, the Costes threshold
457 regression was used as the reference to establish a threshold, and three randomly selected square
458 regions were chosen for each image pair. For each genotype, more than 10 worms were imaged
459 and analyzed. Co-localization analysis was conducted by calculating both Pearson's correlation
460 coefficient (PCC) and Mander's overlap coefficient (MOC) [40].
461

462 **Western blot analysis**

463 For the western blotting experiments, 100 L4-worms were hand-picked into 20 μL
464 ddH_2O, immediately flash-frozen in liquid nitrogen, and kept frozen for more than 30 minutes.
465 Then 5 μL 5×SDS sample buffer (0.2 M Tris·HCl, pH 6.8, 20% glycerol, 10% SDS, 0.25%
466 bromophenol blue, 10% β-mercaptoethanol) was added to each sample. The samples were then
467 boiled at 95°C for 10 min, centrifuged at 13k rpm for 20 min, and stored at -20°C until gel
468 electrophoresis. Proteins were separated using 7.5% Mini-PROTEAN TGX Precast Gels from
469 Bio-Rad Laboratories, Inc., and transferred onto Immobilon-P PVDF membrane
470 (MilliporeSigma) for 9 min under 1.3A and 25V using the Power Blotter Station (Model:
471 PB0010, Invitrogen by Thermo Fisher Scientific). The membrane was incubated in EveryBlot
472 Blocking Buffer (Bio-Rad Laboratories, Inc.) for 5 min at room temperature, and then incubated
473 at 4°C overnight in primary antibodies diluted in EveryBlot Blocking Buffer. Primary antibodies
474 used include mouse anti-FLAG IgG monoclonal antibody (Krackler Scientific; 45-F3165; diluted

475 1:2,000) and mouse anti-actin IgM JLA20 monoclonal antibody (Developmental Studies
476 Hybridoma Bank; diluted 1:2,000). Secondary antibodies used included peroxidase-conjugated
477 donkey anti-mouse IgG and peroxidase-conjugated goat anti-mouse IgM (all from Jackson
478 ImmunoResearch; diluted 1:10,000). Enhanced chemiluminescence was detected using the
479 Western Blotting Luminol Reagent (Santa Cruz Biotechnology; sc-2048). The Bio-Rad
480 ChemiDoc MP imaging system was used to capture the chemiluminescence signal. The western
481 blot experiment was repeated 3 times using different biological samples. Open-source Fiji
482 software was used to quantify western blotting images.
483

484 **Acknowledgements**

485 This paper is dedicated to the memory of the late Herong Shi, a dear friend and a
486 dedicated colleague to many members of the Liu lab. We thank Andy Fire, Bob Goldstein, Barth
487 Grant, Ariel Pani for plasmids or strains, and the rest of the Liu lab for helpful discussions and
488 critical comments on the manuscript.
489

490 **Funding information**

491 This work was supported by NIH R01 GM103869 and R35 GM130351 to JL. Some
492 strains were obtained from the *C. elegans* Genetics Center, which is funded by NIH Office of 27
493 Research Infrastructure Programs (P40 OD010440). The confocal imaging data was acquired
494 through the Cornell University Biotechnology Resource Center, with NYSTEM (CO29155) and
495 NIH (S10OD018516) funding for the shared Zeiss LSM880 confocal/multiphoton microscope.
496

497 **Competing interest**

498 The authors declare that no competing interests exist.

499

500 **References**

501 1. Hemler ME. Tetraspanin functions and associated microdomains. Nature
502 reviewsMolecular cell biology. 2005;6(10):801-11. doi: 10.1038/nrm1736.
503 2. Termini CM, Gillette JM. Tetraspanins Function as Regulators of Cellular Signaling. Front
504 Cell Dev Biol. 2017;5:34. Epub 2017/04/22. doi: 10.3389/fcell.2017.00034. PubMed PMID:
505 28428953; PubMed Central PMCID: PMCPMC5382171.
506 3. Matthews AL, Szyroka J, Collier R, Noy PJ, Tomlinson MG. Scissor sisters: regulation of
507 ADAM10 by the TspanC8 tetraspanins. Biochem Soc Trans. 2017;45(3):719-30. Epub
508 2017/06/18. doi: 10.1042/BST20160290. PubMed PMID: 28620033; PubMed Central PMCID:
509 PMCPMC5473022.
510 4. Saint-Pol J, Eschenbrenner E, Dornier E, Boucheix C, Charrin S, Rubinstein E. Regulation
511 of the trafficking and the function of the metalloprotease ADAM10 by tetraspanins. Biochem
512 Soc Trans. 2017;45(4):937-44. Epub 2017/07/09. doi: 10.1042/BST20160296. PubMed PMID:
513 28687716.
514 5. Dornier E, Coumailleau F, Ottavi JF, Moretti J, Boucheix C, Mauduit P, et al. TspanC8
515 tetraspanins regulate ADAM10/Kuzbanian trafficking and promote Notch activation in flies and
516 mammals. The Journal of cell biology. 2012;199(3):481-96. doi: 10.1083/jcb.201201133 [doi].
517 6. Haining EJ, Yang J, Bailey RL, Khan K, Collier R, Tsai S, et al. The TspanC8 subgroup of
518 tetraspanins interacts with A disintegrin and metalloprotease 10 (ADAM10) and regulates its
519 maturation and cell surface expression. The Journal of biological chemistry.
520 2012;287(47):39753-65. doi: 10.1074/jbc.M112.416503 [doi].
521 7. Prox J, Willenbrock M, Weber S, Lehmann T, Schmidt-Arras D, Schwanbeck R, et al.
522 Tetraspanin15 regulates cellular trafficking and activity of the ectodomain sheddase ADAM10.
523 Cellular and molecular life sciences : CMLS. 2012;69(17):2919-32. doi: 10.1007/s00018-012-
524 0960-2 [doi].
525 8. Koo CZ, Harrison N, Noy PJ, Szyroka J, Matthews AL, Hsia HE, et al. The tetraspanin
526 Tspan15 is an essential subunit of an ADAM10 scissor complex. J Biol Chem.
527 2020;295(36):12822-39. Epub 2020/03/01. doi: 10.1074/jbc.RA120.012601. PubMed PMID:
528 32111735; PubMed Central PMCID: PMCPMC7476718.
529 9. Shah J, Rouaud F, Guerrera D, Vasileva E, Popov LM, Kelley WL, et al. A Dock-and-Lock
530 Mechanism Clusters ADAM10 at Cell-Cell Junctions to Promote alpha-Toxin Cytotoxicity. Cell
531 Rep. 2018;25(8):2132-47 e7. Epub 2018/11/22. doi: 10.1016/j.celrep.2018.10.088. PubMed
532 PMID: 30463011.
533 10. Perez-Martinez CA, Maravillas-Montero JL, Meza-Herrera I, Vences-Catalan F, Zlotnik A,
534 Santos-Argumedo L. Tspan33 is Expressed in Transitional and Memory B Cells, but is not
535 Responsible for High ADAM10 Expression. Scand J Immunol. 2017;86(1):23-30. Epub
536 2017/04/28. doi: 10.1111/sji.12559. PubMed PMID: 28449222.
537 11. Seipold L, Altmeppen H, Koudelka T, Tholey A, Kasparek P, Sedlacek R, et al. In vivo
538 regulation of the A disintegrin and metalloproteinase 10 (ADAM10) by the tetraspanin 15. Cell
539 Mol Life Sci. 2018;75(17):3251-67. Epub 2018/03/10. doi: 10.1007/s00018-018-2791-2.
540 PubMed PMID: 29520422.
541 12. Eschenbrenner E, Jouannet S, Clay D, Chaker J, Boucheix C, Brou C, et al. TspanC8
542 tetraspanins differentially regulate ADAM10 endocytosis and half-life. Life Sci Alliance.

543 2020;3(1). Epub 2019/12/04. doi: 10.26508/lsa.201900444. PubMed PMID: 31792032; PubMed
544 Central PMCID: PMCPMC6892437.
545 13. Dunn CD, Sulis ML, Ferrando AA, Greenwald I. A conserved tetraspanin subfamily
546 promotes Notch signaling in Caenorhabditis elegans and in human cells. Proceedings of the
547 National Academy of Sciences of the United States of America. 2010;107(13):5907-12. doi:
548 10.1073/pnas.1001647107.
549 14. Liu Z, Shi H, Szymczak LC, Aydin T, Yun S, Constas K, et al. Promotion of bone
550 morphogenetic protein signaling by tetraspanins and glycosphingolipids. PLoS Genet.
551 2015;11(5):e1005221. doi: 10.1371/journal.pgen.1005221. PubMed PMID: 25978409; PubMed
552 Central PMCID: PMCPMC4433240.
553 15. Wang L, Liu Z, Shi H, Liu J. Two Paralogous Tetraspanins TSP-12 and TSP-14 Function
554 with the ADAM10 Metalloprotease SUP-17 to Promote BMP Signaling in Caenorhabditis
555 elegans. PLoS Genet. 2017;13(1):e1006568. doi: 10.1371/journal.pgen.1006568. PubMed PMID:
556 28068334; PubMed Central PMCID: PMCPMC5261805.
557 16. Liu Z, Shi H, Nzessi AK, Norris A, Grant BD, Liu J. Tetraspanins TSP-12 and TSP-14 function
558 redundantly to regulate the trafficking of the type II BMP receptor in Caenorhabditis elegans.
559 Proc Natl Acad Sci U S A. 2020;117(6):2968-77. Epub 2020/01/29. doi:
560 10.1073/pnas.1918807117. PubMed PMID: 31988138; PubMed Central PMCID:
561 PMCPMC7022192.
562 17. Savage-Dunn C, Padgett RW. The TGF-beta Family in Caenorhabditis elegans. Cold Spring
563 Harb Perspect Biol. 2017;9(6). doi: 10.1101/cshperspect.a022178. PubMed PMID: 28096268;
564 PubMed Central PMCID: PMCPMC5453393.
565 18. Frokjaer-Jensen C, Davis MW, Hopkins CE, Newman BJ, Thummel JM, Olesen SP, et al.
566 Single-copy insertion of transgenes in Caenorhabditis elegans. Nat Genet. 2008;40(11):1375-83.
567 Epub 2008/10/28. doi: 10.1038/ng.248. PubMed PMID: 18953339; PubMed Central PMCID:
568 PMCPMC2749959.
569 19. Traub LM, Bonifacino JS. Cargo recognition in clathrin-mediated endocytosis. Cold Spring
570 Harb Perspect Biol. 2013;5(11):a016790. Epub 2013/11/05. doi: 10.1101/cshperspect.a016790.
571 PubMed PMID: 24186068; PubMed Central PMCID: PMCPMC3809577.
572 20. Bonifacino JS, Traub LM. Signals for sorting of transmembrane proteins to endosomes
573 and lysosomes. Annu Rev Biochem. 2003;72:395-447. Epub 2003/03/26. doi:
574 10.1146/annurev.biochem.72.121801.161800. PubMed PMID: 12651740.
575 21. Rudnicki MA, Braun T, Hinuma S, Jaenisch R. Inactivation of MyoD in mice leads to up-
576 regulation of the myogenic HLH gene Myf-5 and results in apparently normal muscle
577 development. Cell. 1992;71(3):383-90. doi: 0092-8674(92)90508-A [pii].
578 22. Wang Y, Schnegelsberg PN, Dausman J, Jaenisch R. Functional redundancy of the
579 muscle-specific transcription factors Myf5 and myogenin. Nature. 1996;379(6568):823-5. Epub
580 1996/02/29. doi: 10.1038/379823a0. PubMed PMID: 8587605.
581 23. Shim J, Sternberg PW, Lee J. Distinct and redundant functions of mu1 medium chains of
582 the AP-1 clathrin-associated protein complex in the nematode Caenorhabditis elegans. Mol Biol
583 Cell. 2000;11(8):2743-56. Epub 2000/08/10. doi: 10.1091/mbc.11.8.2743. PubMed PMID:
584 10930467; PubMed Central PMCID: PMCPMC14953.

585 24. Shafaq-Zadah M, Brocard L, Solari F, Michaux G. AP-1 is required for the maintenance of
586 apico-basal polarity in the C. elegans intestine. Development. 2012;139(11):2061-70. Epub
587 2012/04/27. doi: 10.1242/dev.076711. PubMed PMID: 22535414.
588 25. Zhang H, Kim A, Abraham N, Khan LA, Hall DH, Fleming JT, et al. Clathrin and AP-1
589 regulate apical polarity and lumen formation during C. elegans tubulogenesis. Development.
590 2012;139(11):2071-83. Epub 2012/04/27. doi: 10.1242/dev.077347. PubMed PMID: 22535410;
591 PubMed Central PMCID: PMCPMC3347694.
592 26. Pan CL, Baum PD, Gu M, Jorgensen EM, Clark SG, Garriga G. C. elegans AP-2 and
593 retromer control Wnt signaling by regulating mig-14/Wntless. Dev Cell. 2008;14(1):132-9. Epub
594 2007/12/28. doi: 10.1016/j.devcel.2007.12.001. PubMed PMID: 18160346; PubMed Central
595 PMCID: PMCPMC2709403.
596 27. Saint-Pol J, Billard M, Dornier E, Eschenbrenner E, Danglot L, Boucheix C, et al. New
597 insights into the tetraspanin Tspan5 using novel monoclonal antibodies. J Biol Chem.
598 2017;292(23):9551-66. Epub 2017/04/22. doi: 10.1074/jbc.M116.765669. PubMed PMID:
599 28428248; PubMed Central PMCID: PMCPMC5465482.
600 28. Savage-Dunn C, Gleason RJ, Liu J, Padgett RW. Mutagenesis and Imaging Studies of BMP
601 Signaling Mechanisms in C. elegans. Methods Mol Biol. 2019;1891:51-73. Epub 2018/11/11.
602 doi: 10.1007/978-1-4939-8904-1_6. PubMed PMID: 30414126; PubMed Central PMCID:
603 PMCPMC6731545.
604 29. Berditchevski F, Odintsova E. Tetraspanins as regulators of protein trafficking. Traffic.
605 2007;8(2):89-96. Epub 2006/12/22. doi: 10.1111/j.1600-0854.2006.00515.x. PubMed PMID:
606 17181773.
607 30. Kummer D, Steinbacher T, Schwietzer MF, Tholmann S, Ebnet K. Tetraspanins:
608 integrating cell surface receptors to functional microdomains in homeostasis and disease. Med
609 Microbiol Immunol. 2020;209(4):397-405. Epub 2020/04/11. doi: 10.1007/s00430-020-00673-3.
610 PubMed PMID: 32274581; PubMed Central PMCID: PMCPMC7395057.
611 31. van Deventer S, Arp AB, van Spriel AB. Dynamic Plasma Membrane Organization: A
612 Complex Symphony. Trends Cell Biol. 2021;31(2):119-29. Epub 2020/11/30. doi:
613 10.1016/j.tcb.2020.11.004. PubMed PMID: 33248874.
614 32. Zoller M. Tetraspanins: push and pull in suppressing and promoting metastasis. Nature
615 reviewsCancer. 2009;9(1):40-55. doi: 10.1038/nrc2543 [doi].
616 33. Hemler ME. Tetraspanin proteins promote multiple cancer stages. Nature
617 reviewsCancer. 2014;14(1):49-60.
618 34. Harrison N, Koo CZ, Tomlinson MG. Regulation of ADAM10 by the TspanC8 Family of
619 Tetraspanins and Their Therapeutic Potential. Int J Mol Sci. 2021;22(13). Epub 2021/07/03. doi:
620 10.3390/ijms22136707. PubMed PMID: 34201472; PubMed Central PMCID: PMCPMC8268256.
621 35. Tian C, Shi H, Xiong S, Hu F, Xiong WC, Liu J. The neogenin/DCC homolog UNC-40
622 promotes BMP signaling via the RGM protein DRAG-1 in C. elegans. Development (Cambridge,
623 England). 2013;140(19):4070-80. doi: 10.1242/dev.099838 [doi].
624 36. Arribere JA, Bell RT, Fu BX, Artiles KL, Hartman PS, Fire AZ. Efficient marker-free recovery
625 of custom genetic modifications with CRISPR/Cas9 in Caenorhabditis elegans. Genetics.
626 2014;198(3):837-46. Epub 2014/08/28. doi: 10.1534/genetics.114.169730. PubMed PMID:
627 25161212; PubMed Central PMCID: PMCPMC4224173.

628 37. Dickinson DJ, Pani AM, Heppert JK, Higgins CD, Goldstein B. Streamlined Genome
629 Engineering with a Self-Excising Drug Selection Cassette. Genetics. 2015;200(4):1035-49. Epub
630 2015/06/06. doi: 10.1534/genetics.115.178335. PubMed PMID: 26044593; PubMed Central
631 PMCID: PMCPMC4574250.
632 38. Pani AM, Goldstein B. Direct visualization of a native Wnt in vivo reveals that a long-
633 range Wnt gradient forms by extracellular dispersal. Elife. 2018;7. Epub 2018/08/15. doi:
634 10.7554/eLife.38325. PubMed PMID: 30106379; PubMed Central PMCID: PMCPMC6143344.
635 39. Schindelin J, Arganda-Carreras I, Frise E, Kaynig V, Longair M, Pietzsch T, et al. Fiji: an
636 open-source platform for biological-image analysis. Nat Methods. 2012;9(7):676-82. doi:
637 10.1038/nmeth.2019. PubMed PMID: 22743772; PubMed Central PMCID: PMCPMC3855844.
638 40. Aaron JS, Taylor AB, Chew TL. Image co-localization - co-occurrence versus correlation. J
639 Cell Sci. 2018;131(3). Epub 2018/02/14. doi: 10.1242/jcs.211847. PubMed PMID: 29439158.
640

641 **Figure legends**

642 **Figure 1. The two TSP-14 isoforms: TSP-14A and TSP-14B.**

643 **(A).** Schematic representation of the *tsp-14* locus, showing only the alternative and shared
644 coding exons of *tsp-14a* and *tsp-14b*. Exons are represented by boxes, and introns by lines. ATG
645 represents the start codon of each isoform. The first coding exon for *tsp-14b* is located 3511bp
646 upstream of the first coding exon of *tsp-14a*. (**B).** A schematic of TSP-14A and TSP-14B
647 proteins, showing the four transmembrane domains, and the various extracellular and
648 intracellular regions. The only difference between TSP-14A and TSP-14B is at their N-termini,
649 with the red line representing the extra amino acids present in TSP-14B. The CCG and CC
650 motifs in the second extracellular loop are represented by solid circles, with orange solid circle
651 representing cysteine, while the yellow solid circle representing glycine. PM, plasma membrane.
652 Ext, extracellular. (**C).** Alignment of the amino acid sequences of TSP-14A and TSP-14B. TSP-
653 14B has 24 additional amino acids at its N-terminus (red), which includes the ExxLL motif
654 (blue). The four transmembrane domains are indicated in green and the cysteine residues in the
655 extracellular domain are in red.

656

657 **Figure 2. Isoform-specific knockouts of TSP-14 cause distinct phenotypes.**

658 **(A).** Schematics of the *tsp-14* locus, showing isoform-specific knockouts generated in this study.
659 In *jj304,* the TSP-14A start codon ATG (methionine) is mutated to TTG (isoleucine), knocking
660 out TSP-14A, while introducing a single, although conserved amino acid change in TSP-14B.
661 The *tsp-14(jj304)* allele is also referred to as *tsp-14a(0)*. In *jj317*, the TSP-14B start codon ATG
662 and a downstream, in-frame, ATG (see Figure 1C) are mutated to TTG and TTA respectively,
663 knocking out TSP-14B without affecting TSP-14A. The *tsp-14(jj317)* allele is also referred to as

664 *tsp-14b(0)*. (**B).** Relative body lengths of synchronized L4 worms of various genotypes. The
665 mean body length of wild-type worms is normalized to 1.0. Numbers within each bar indicate the
666 total number of worms measured. For each double mutant, data were pooled from two
667 independent isolates. Error bars represent 95% confidence interval (C.I.). Tukey's honestly
668 significant difference (HSD) test following an ANOVA was used to test for differences between
669 different genotypes. ***$P < 0.0001$. n.s., no significant difference. WT: wild-type. *tsp-12(0)*: *tsp-*
670 *12(jj300)*. *tsp-14(0)*: *tsp-14(jj95)*. *tsp-14a(0)*: *tsp-14(jj304)*. *tsp-14b(0)*: *tsp-14(jj317)*. (**C-N).**
671 Differential interference contrast (DIC) micrographs of wild-type (WT, C-E), *tsp-12(0); tsp-*
672 *14(0)* (F-H)*, tsp-12(0); tsp-14a(0)* (I-K)*, tsp-12(0); tsp-14b(0)* (L-N) animals at the L4 (C, F, I,
673 L) or young adult stage (D, G, J, M), or their embryos at mid-embryogenesis (E, H, K, N). L4,
674 L4 larva. YA, young adult. Scale bars represent 20 µm. **(O).** Diagrams depicting the *sma-9(0)*
675 suppression (Susm) assay. Mutations in the BMP pathway can suppress the loss of M-lineage-
676 derived coelomocytes (CCs) in *sma-9(0)* mutants. CCs are depicted as green circles. **P**). Table
677 summarizing the results of the *sma-9(0)* suppression assay of various *tsp-14* alleles. Percentage
678 of suppression was calculated by the number of worms with 1-2 M-derived CCs divided by the
679 total number of worms scored. N represents the total number of worms counted. Data from two
680 independent isolates were combined for each genotype. * The loss of M-derived CCs phenotype
681 of *sma-9(cc604)* null mutants is not fully penetrant.
682
683 **Figure 3. TSP-14A and TSP-14B have distinct and shared functions.**
684 **(A)** Schematics depicting the single copy transgenes expressing either *tsp-14a* or *tsp-14b* under
685 the 3.3kb or 5.2kb *tsp-14* promoter at the *ttTi4348* locus on chromosome I. **(B)** Table
686 summarizing the results of the *sma-9(0)* suppression assay when *tsp-14a* or *tsp-14b* was

687 expressed as a single copy transgene. Percentage of suppression was calculated by the number of
688 worms with 1-2 M-derived CCs divided by the total number of worms scored. * The loss of M-
689 derived CCs phenotype of *sma-9(cc604)* null mutants is not fully penetrant**. (C)** Relative body
690 lengths of synchronized L4 worms of various genotypes at the Christmas tree stage. The mean
691 body length of wild-type (WT) worms is normalized to 1.0. Numbers within each bar indicate
692 the total number of worms measured. For each double mutant, data were pooled from two
693 independent isolates. Error bars represent 95% C.I. Tukey's HSD test following an ANOVA was
694 used to test for differences between different genotypes. ***$P < 0.0001$. WT: wild-type. *tsp-*
695 *12(0)*: *tsp-12(jj300)*. *tsp-14(0)*: *tsp-14(jj95)*.
696
697 **Figure 4. Endogenous TSP-14A ad TSP-14B can be respectively and functionally tagged.**
698 **(A).** Schematic representations of wild-type and GFP-tagged TSP-14 isoforms. In *jj192* animals,
699 TSP-14B is specifically tagged at its N-terminus with GFP::3xFLAG. In *jj183* animals, TSP-14A
700 specifically tagged at its N-terminus with GFP::3xFLAG. However, if spliced properly, the tag is
701 also inserted into TSP-14B after the first 24aa. Both TSP-14A and TSP-14B are tagged at their
702 C-termini with GFP::3xFLAG in *jj219* animals. The same GFP::3xFLAG tag as in *jj219* is also
703 in *jj304 jj319* and *jj317 jj377* animals when one of the respective *tsp-14* isoforms is knocked out.
704 (**B).** Relative body lengths of synchronized L4 worms of various genotypes. The mean body
705 length of wild-type worms is normalized to 1.0. Numbers within each bar indicate the total
706 number of worms measured. For each double mutant, data were pooled from two independent
707 isolates. Error bars represent 95% C.I. Tukey's HSD test following an ANOVA was used to test
708 for differences between different genotypes. ***$P < 0.0001$. n.s., no significant difference. As
709 shown, *tsp-12(0); tsp-14(jj192)* worms are slightly smaller than wild-type (WT) worms, but not

710 as small as *tsp-12(0); tsp-14(jj95)* worms. (**C).** Tables summarizing the results of the *sma-9(0)*
711 suppression assay of various *tsp-14* alleles, in combination with the *tsp-12(jj300)* null allele.
712 Percentage of suppression was calculated by the number of worms with 1-2 M-derived CCs
713 divided by the total number of worms scored. N represents the total number of worms counted.
714 Data from two independent isolates were combined for each genotype. * The loss of M-derived
715 CCs phenotype of *sma-9(cc604)* null mutants is not fully penetrant. (**D).** Western blot showing
716 the various tagged forms of TSP-14A and/or TSP-14B detected by anti-FLAG antibodies. Anti-
717 actin antibodies were used as a loading control. For each lane, 100 synchronized L4 animals
718 were used to prepare the samples. The genotypes of *jj322 jj192* and *jj368 jj378* are described in
719 Figure 7.
720
721 **Figure 5. TSP-14A and TSP-14B exhibit distinct localization patterns.**
722 (**A-M**) Airyscan confocal images showing the localization of TSP-14A (A-C' and E), TSP-14B
723 (F-G' and I), and both TSP-14A and TSP-14B (J-K' and M) in the head region (GFP: A, F, J,
724 and DIC: A', F', J'), hypodermal cells (GFP: C, G, K, and DIC: C', G', K'), and the developing
725 vulva (E, I, and M). GFP::TSP-14A is detectable in the tips of anterior sensory cilia (arrow in A),
726 and in sperm cells (arrows in B). * in A and B marks autofluorescence signals. Scale bar in A-M,
727 10 µm. Panels D, E and L are schematic representations of the different knock-ins. (**O-W**)
728 Airyscan confocal GFP (O, P, R, S, U, V) and corresponding DIC (O', P', R', S', U', V') images
729 of the developing vulva (O, R, U) and hypodermal cells (P, S, V) from worms expressing
730 different tagged versions of TSP-14. Panels Q, T and W are schematic representations of the
731 different knock-ins. Scale bars in O-W, 20 µm.
732

733 **Figure 6. TSP-14A is co-localized with TSP-12 and is localized to endosomes.**

734 (**A)** Schematics of GFP- or TagRFP-tagged TSP-14A. (**B-G**) Airyscan confocal images of late
735 L4 hypodermal cells expressing both tagged TSP-14A (B, GFP-tagged TSP-14A and E,
736 TagRFP-tagged TSP-14A) and tagged TSP-12 (C, TagRFP-tagged TSP-12 and F, GFP-tagged
737 TSP-12). The corresponding merged images are shown in D and G, respectively. (**H**) The
738 colocalization between TSP-14A and TSP-12 was quantified using two different methods. PCC,
739 Pearson's correlation coefficient; MOC, Mander's overlap coefficient. PCC indicates the
740 correlation of GFP::TSP-14A with TagRFP::TSP-12 or TagRFP::TSP-14A with GFP::TSP-12.
741 MOC indicates the fraction of TagRFP::TSP-12 that overlaps with GFP::TSP-14A (the second
742 bar), or the fraction of GFP::TSP-12 that overlaps with TagRFP::TSP-14A (the forth bar). (**I-Q**)
743 Airyscan confocal images of L4 stage hypodermal cells expressing N-terminally GFP-tagged
744 TSP-14A (J, M, P) and different endosomal markers, TagRFP::EEA-1 (I, early endosomes),
745 TagRFP::RAB-7 (L, late endosomes), and TagRFP::RAB-11 (O, recycling endosomes). K, N
746 and Q are the corresponding merged images. **(R)** Bar graphics showing the correlation of
747 TagRFP (EEA-1, RAB-7 or RAB-11) with GFP::TSP-14A (PCC), and the fraction of TSP-
748 14A::GFP that overlaps with TagRFP (MOC). Error bars in H and R represent SEM. Statistical
749 analysis was done using a 2-tailed *t* test with 95% CIs. Scale bar, 5 µm.

750

751 **Figure 7. TSP-14B is sufficient to localize to the basolateral membrane upon forced**
752 **expression.**

753 Airyscan confocal images of L4 worms expressing either TSP-14A (**A**) or TSP-14B (**B**) in the
754 *tsp-14(0)* background under the *snx-1* promoter as single copy transgenes in the *ttTi4348* locus
755 on chromosome I. Images shown are of the head region and intestine cells. Arrows point to TSP-

756 14A or TSP-14B signals. Asterisks mark intestinal autofluorescence. TSP-14B::GFP is
757 concentrated on the membrane in the head region and in the basolateral membrane of the
758 intestinal cells, while the TSP-14A::GFP signal is not detectable on cell membranes. Scale bars,
759 20 µm.
760
761 **Figure 8. The 24aa unique to TSP-14B contains a basolateral membrane targeting**
762 **sequence.**
763 **(A, B, E)** Schematics of the wild-type (WT) and *jj368* mutant *tsp-14* loci, either untagged (A), or
764 N-terminally GFP-tagged (B, E), showing the EQCLL sequence in WT TSP-14B (or in *jj192*, B)
765 mutated to AQCAA in *jj368* (A) or *jj322 jj192* (E). (**C-D, F-G)** Airyscan confocal images of L4
766 larvae showing that wild-type (WT) TSP-14B is localized to the basolateral membrane in the
767 developing vulva (C) and in hypodermal cells (D), while mutated TSP-14B carrying the AQCAA
768 mutation is localized to the apical side of the developing vulva (F) and in intracellular vesicles in
769 hypodermal cells (G). Scale bars, 10 µm. (**H**) Relative body lengths of synchronized L4 worms
770 at the Christmas tree stage. The mean body length of wild-type worms is normalized to 1.0. For
771 each double mutant, data were pooled from two independent isolates. Numbers within each bar
772 indicate the total number of worms measured. Error bars represent 95% C.I. Tukey's HSD
773 following an ANOVA was used to test for differences between different genotypes. ***$P <$
774 0.0001. WT: wild-type. *tsp-12(0)*: *tsp-12(jj300)*. *tsp-14(0)*: *tsp-14(jj95)*. As shown, *tsp-12(0);*
775 *tsp-14(jj368)* worms are slightly smaller than WT worms, but not as small as *tsp-12(0); tsp-*
776 *14(jj95)* worms. (**I**) Table summarizing the results of the *sma-9(0)* suppression assay. Percentage
777 of suppression was calculated by the number of worms with 1-2 M-derived CCs divided by the
778 total number of worms scored. N represents the total number of worms counted. Data from two

independent isolates were combined for each genotype. * The loss of M-derived CCs phenotype of *sma-9(cc604)* null mutants is not fully penetrant. (**J**) Graph summarizing the brood sizes of different strains. *tsp-12(0)*, *tsp-14(0)* and *tsp-14(jj368)* single mutants have the same brood size as wild-type (WT) worms, while *tsp-12(0); tsp-14(0)* and *tsp-12(0); tsp-14(jj368)* double mutants have significant reduced brood sizes compared to WT. *tsp-12(0)*: *tsp-12(jj300)*. *tsp-14(0)*: *tsp-14(jj95)*. Error bars represent 95% C.I. Tukey's HSD following an ANOVA was used to test the differences between different genotypes. ***$P < 0.0001$. (**K**) Schematic representations of the N-terminally GFP-tagged TSP-14A and N-terminally GFP-tagged TSP-14A with EQCLL mutated to AQCAA (*jj368 jj378*). (L) Airyscan confocal images of L4 larvae showing the developing vulva and hypodermal cells. The GFP signal in *jj368 jj378* worms is very faint and not localized to the basolateral cell membrane. Scale bars, 10 µm.

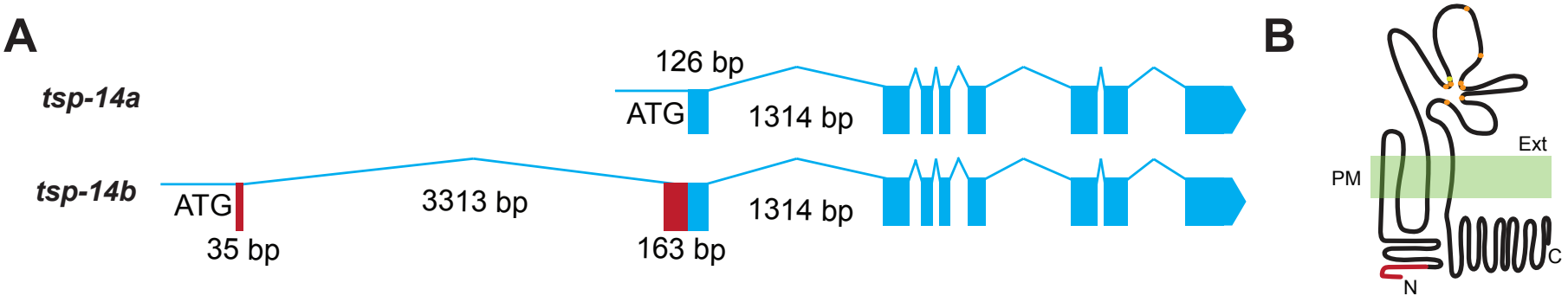

C

```
                    24AA                                                                  TM1
TSP-14A   1 ------------------------MGSGEPTRARAVVSSSHKQRKPRQEISACLKWLVFLLNSIVFLVGVGILALGVYLF 56
TSP-14B   1 MPHRAPRRFMKTAPGACDWEQCLLMGSGEPTRARAVVSSSHKQRKPRQEISACLKWLVFLLNSIVFLVGVGILALGVYLF 80
                                TM2                                   TM3
TSP-14A  57 IKDFREVKLVDIILNPAILISIFGFSICVVSFFGFMGALRDNIFLLKCFAACVFLSYILVVAVTLVFFTLFYTDTTEGLS 136
TSP-14B  81 IKDFREVKLVDIILNPAILISIFGFSICVVSFFGFMGALRDNIFLLKCFAACVFLSYILVVAVTLVFFTLFYTDTTEGLS 160

TSP-14A 137 ANWLLLYAVKNYHTNRNLAEIMDALQENLECCGVSSIAQGYRDWNMSYQFNCTNSNPQPEKCGVPFSCCRKSVISEAAGS 216
TSP-14B 161 ANWLLLYAVKNYHTNRNLAEIMDALQENLECCGVSSIAQGYRDWNMSYQFNCTNSNPQPEKCGVPFSCCRKSVISEAAGS 240
                                                                          TM4
TSP-14A 217 SNPLLPAMRSLECWQNALTKRPGDLEHDIYTRGCLQPLRTLFESHAVHVGAFVALLIVPVCISVCLTNILAKQVDHQRYL 296
TSP-14B 241 SNPLLPAMRSLECWQNALTKRPGDLEHDIYTRGCLQPLRTLFESHAVHVGAFVALLIVPVCISVCLTNILAKQVDHQRYL 320

TSP-14A 297 LEREARRNDRRRKRDHNRRDQLNSLDLLEEGKFNNASANATRPRPPDIPPPLPPIEHVPRKKSRNASSSPTRKPKSAGVE 376
TSP-14B 321 LEREARRNDRRRKRDHNRRDQLNSLDLLEEGKFNNASANATRPRPPDIPPPLPPIEHVPRKKSRNASSSPTRKPKSAGVE 400

TSP-14A 377 NAAARRKRTATTTRTPPAAAGPAPTPQATTTNRTHQWVLQQTDLVPQKSKS 427
TSP-14B 401 NAAARRKRTATTTRTPPAAAGPAPTPQATTTNRTHQWVLQQTDLVPQKSKS 451
```

Figure 1

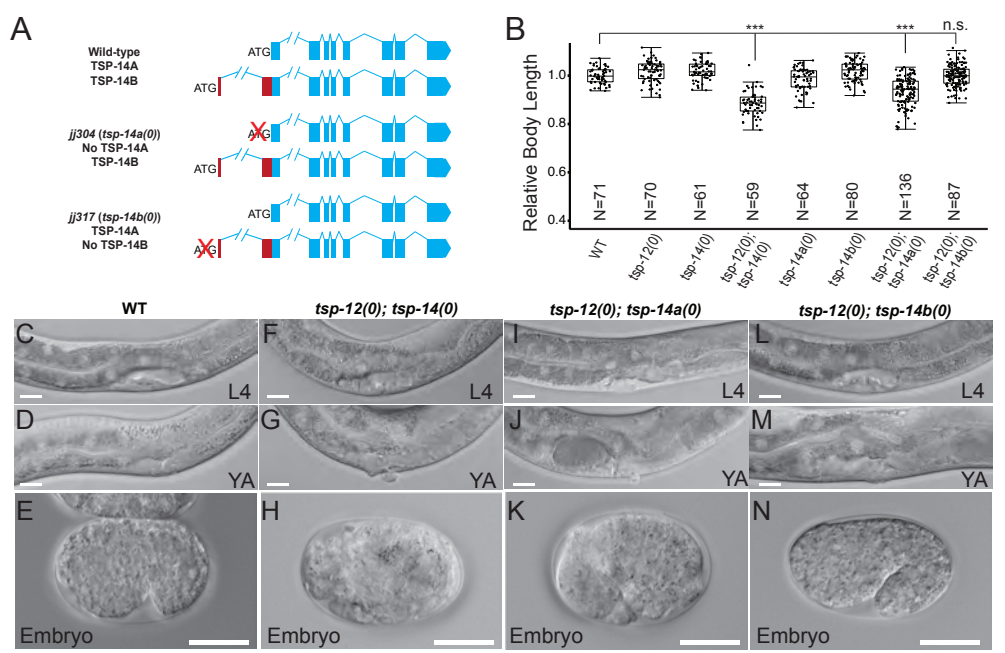

O

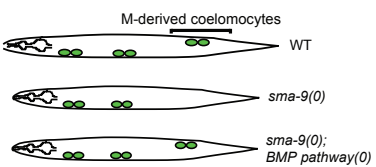

P

Genotype	Suppression(%)	N
sma-9(cc604)	1.4±0.2*	1359
tsp-12(jj300); sma-9(cc604)	16.5±0.8	3343
tsp-14(jj95) sma-9(cc604)	1.9±0.3	2347
tsp-12(jj300); tsp-14(jj95) sma-9(cc604)	80.0±1.3	3952
tsp-14(jj304) sma-9(cc604)	2.0±0.3	1274
tsp-12(jj300); tsp-14(jj304) sma-9(cc604)	19.4±1.9	1938
tsp-14(jj317) sma-9(cc604)	5.4±0.6	958
tsp-12(jj300); tsp-14(jj317) sma-9(cc604)	37.0±2.9	1413

Figure 2

A

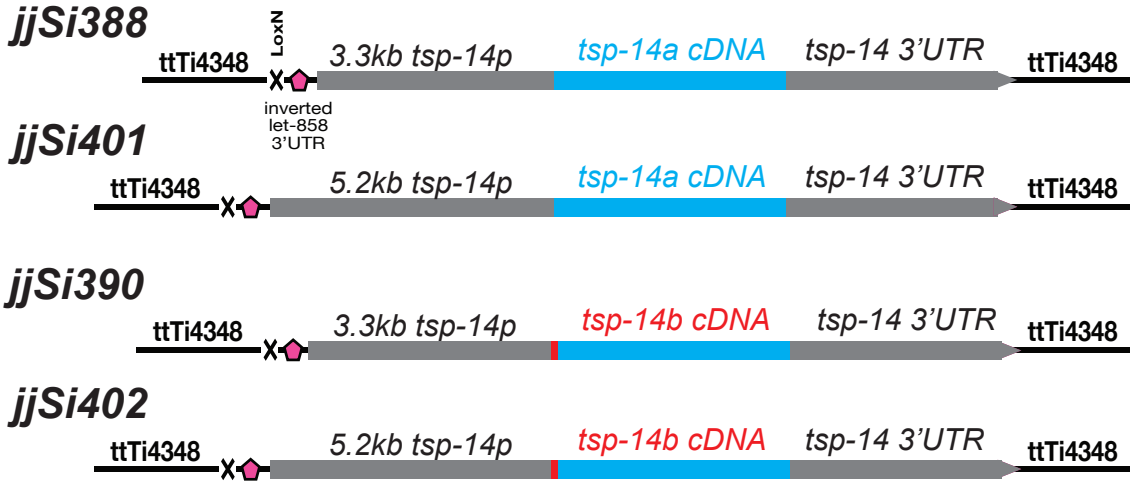

B

Genotype	Suppression(%)	N
sma-9(cc604)	1.3±0.3*	834
tsp-12(jj300); tsp-14(jj95) sma-9(cc604)	79.9±6.5	900
tsp-12(jj300); tsp-14(jj95) sma-9(cc604); jjSi388	79.2±6.7	873
tsp-12(jj300); tsp-14(jj95) sma-9(cc604); jjSi401	76.9±6.2	522
tsp-12(jj300); tsp-14(jj95) sma-9(cc604); jjSi390	55.2±7.8	707
tsp-12(jj300); tsp-14(jj95) sma-9(cc604); jjSi402	46.2±9.5	648

C

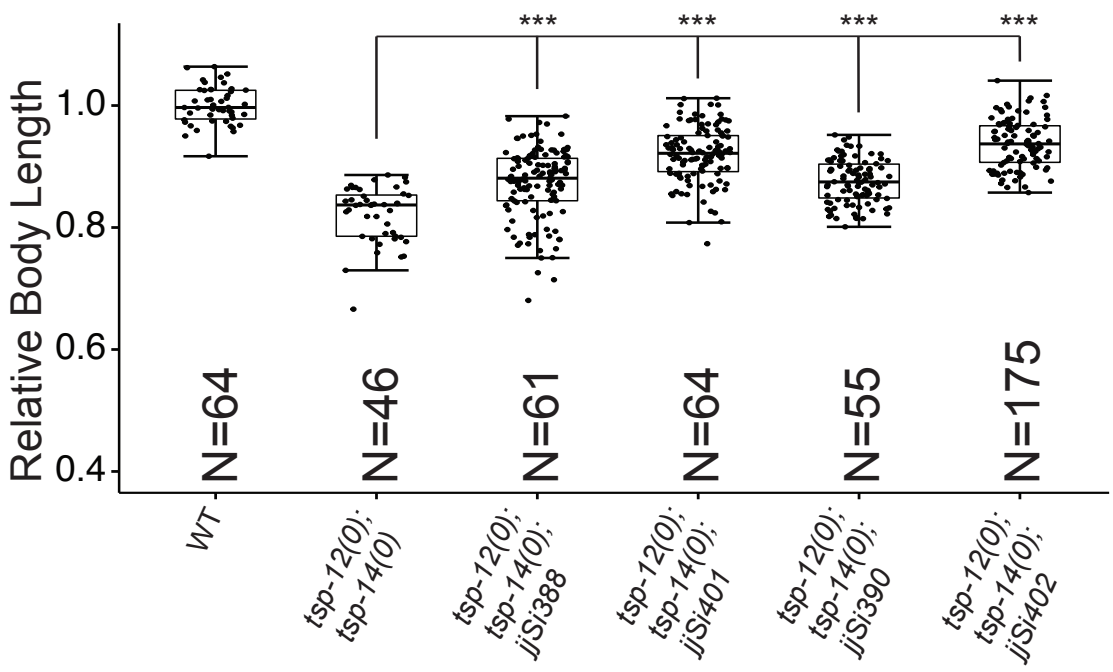

Figure 3

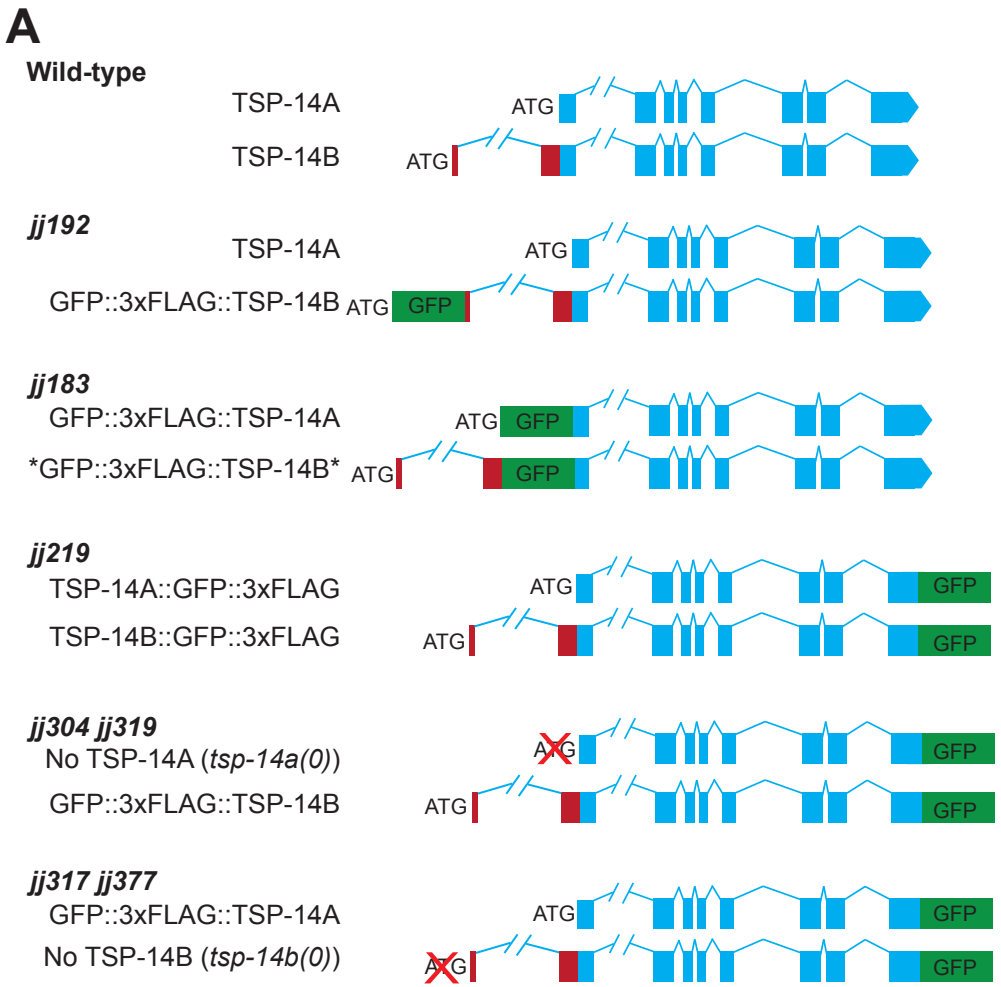

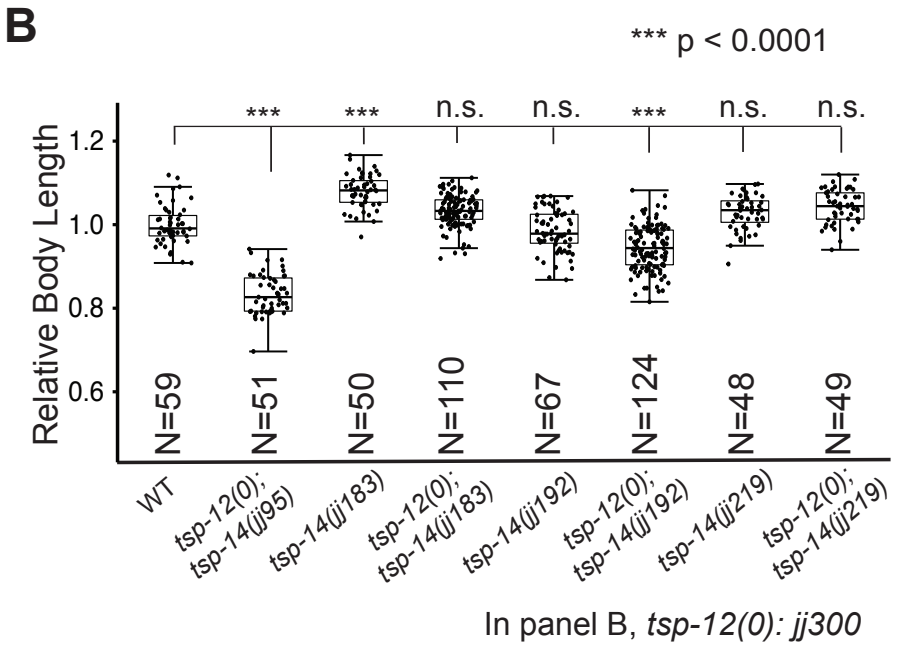

C

Genotype	Suppression(%)	N
sma-9(cc604)	1.5±0.2*	1359
tsp-12(jj300); sma-9(cc604)	16.5±0.8	3343
tsp-14(jj95) sma-9(cc604)	1.9±0.3	2347
tsp-12(jj300); tsp-14(jj95) sma-9(cc604)	80.0±1.3	3952
tsp-14(jj183) sma-9(cc604)	1.9±0.1	2808
tsp-12(jj300); tsp-14(jj183) sma-9(cc604)	20.8±0.8	2979
tsp-14(jj192) sma-9(cc604)	0.7±0.1	3327
tsp-12(jj300); tsp-14(jj192) sma-9(cc604)	2.4±0.4	2140

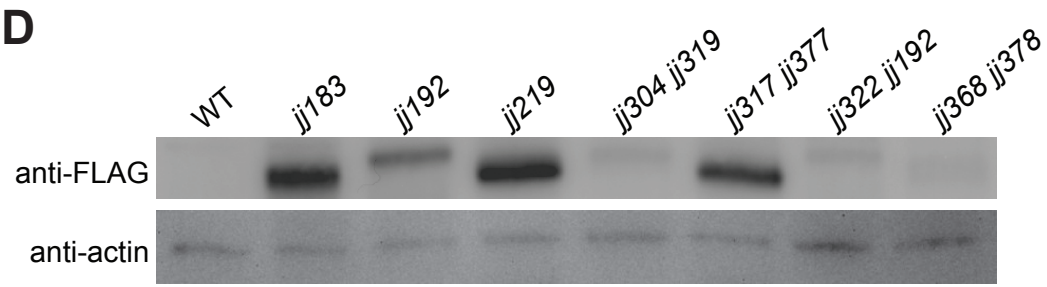

Figure 4

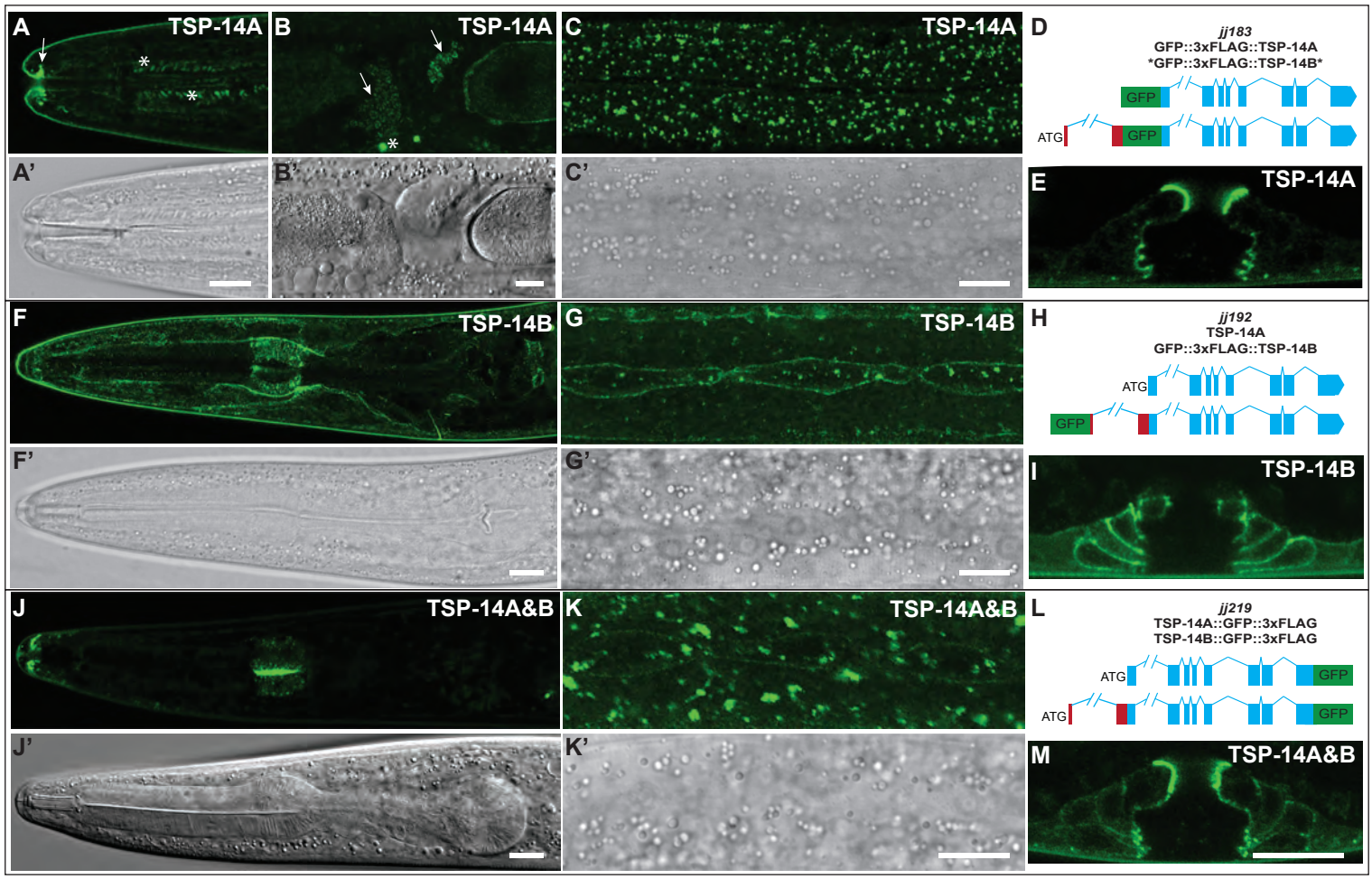
A
TSP-14A
B
TSP-14A
C
TSP-14A
D
jj183
GFP::3xFLAG::TSP-14A
GFP::3xFLAG::TSP-14B
GFP
ATG
GFP
A'
B'
C'
E
TSP-14A
F
TSP-14B
G
TSP-14B
H
jj192
TSP-14A
GFP::3xFLAG::TSP-14B
ATG
GFP
F'
G'
I
TSP-14B
J
TSP-14A&B
K
TSP-14A&B
L
jj219
TSP-14A::GFP::3xFLAG
TSP-14B::GFP::3xFLAG
ATG
GFP
ATG
GFP
J'
K'
M
TSP-14A&B

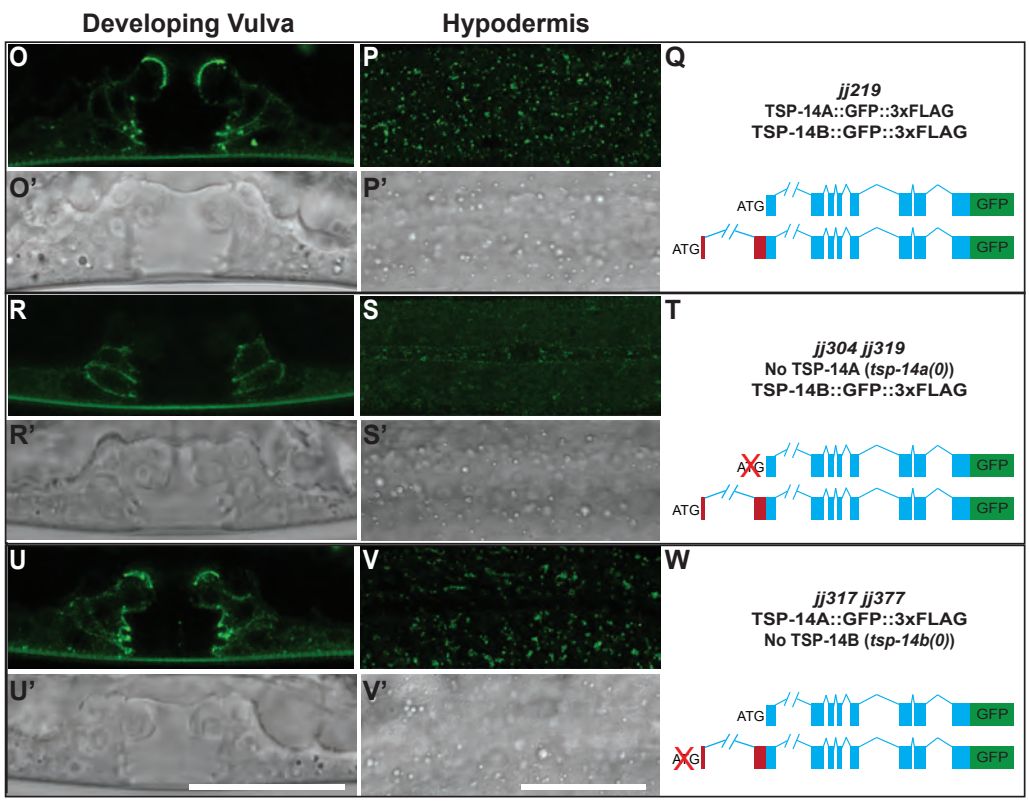
Developing Vulva
Hypodermis
O
P
Q
jj219
TSP-14A::GFP::3xFLAG
TSP-14B::GFP::3xFLAG
ATG
GFP
ATG
GFP
O'
P'
R
S
T
jj304 jj319
No TSP-14A (tsp-14a(0))
TSP-14B::GFP::3xFLAG
ATG
GFP
ATG
GFP
R'
S'
U
V
W
jj317 jj377
TSP-14A::GFP::3xFLAG
No TSP-14B (tsp-14b(0))
ATG
GFP
ATG
GFP
U'
V'

Figure 5

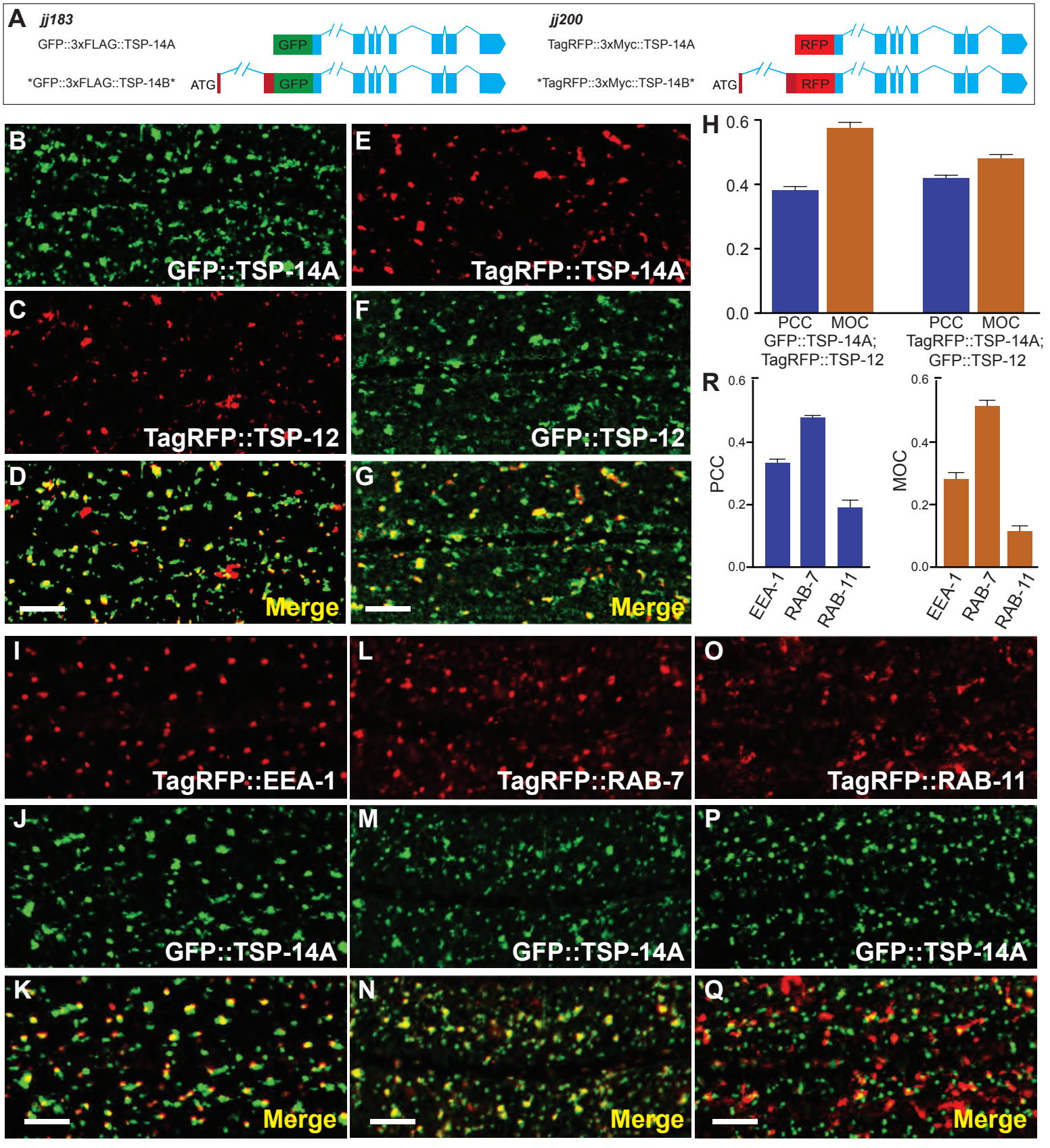
A
jj183
GFP::3xFLAG::TSP-14A
GFP::3xFLAG::TSP-14B
ATG
GFP
GFP
jj200
TagRFP::3xMyc::TSP-14A
TagRFP::3xMyc::TSP-14B
ATG
RFP
RFP
B
GFP::TSP-14A
E
TagRFP::TSP-14A
C
TagRFP::TSP-12
F
GFP::TSP-12
D
Merge
G
Merge
H
0.6
0.4
0.2
0.0
PCC
MOC
GFP::TSP-14A;
TagRFP::TSP-12
PCC
MOC
TagRFP::TSP-14A;
GFP::TSP-12
R
PCC
MOC
EEA-1
RAB-7
RAB-11
I
TagRFP::EEA-1
L
TagRFP::RAB-7
O
TagRFP::RAB-11
J
GFP::TSP-14A
M
GFP::TSP-14A
P
GFP::TSP-14A
K
Merge
N
Merge
Q
Merge

Figure 6

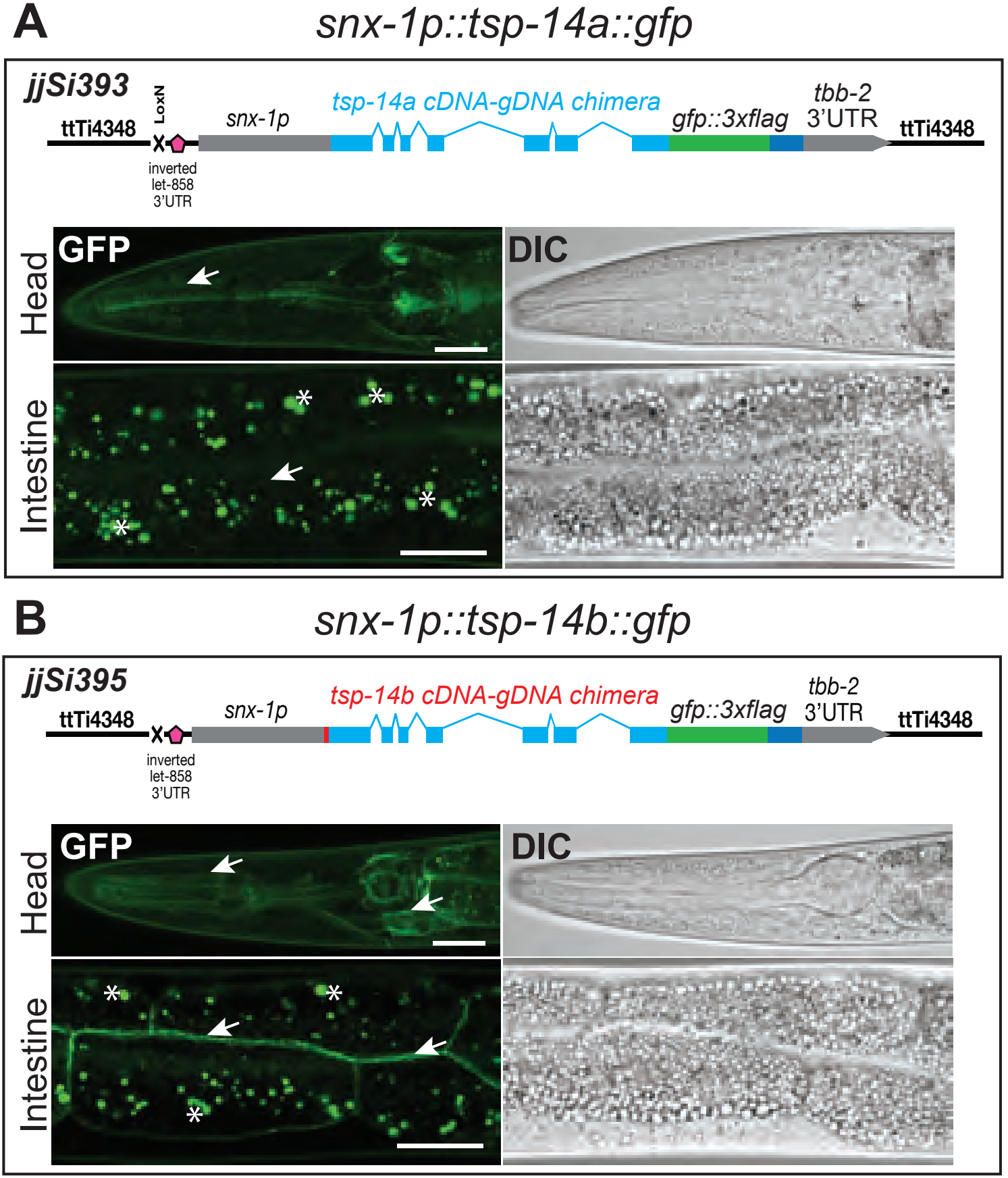
A
snx-1p::tsp-14a::gfp
jjSi393
ttTi4348
LoxN
inverted
let-858
3'UTR
snx-1p
tsp-14a cDNA-gDNA chimera
gfp::3xflag
tbb-2
3'UTR
ttTi4348
Head
Intestine
GFP
DIC
B
snx-1p::tsp-14b::gfp
jjSi395
ttTi4348
inverted
let-858
3'UTR
snx-1p
tsp-14b cDNA-gDNA chimera
gfp::3xflag
tbb-2
3'UTR
ttTi4348
Head
Intestine
GFP
DIC

Figure 7

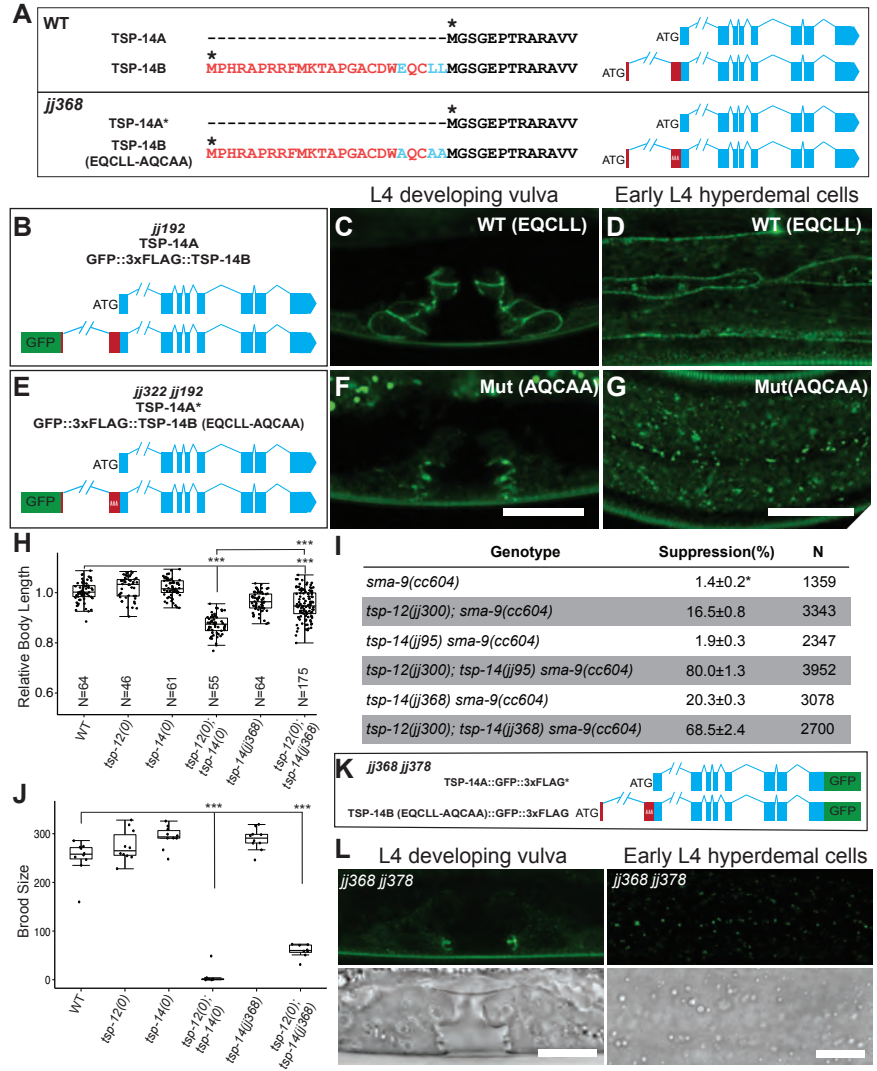

Genotype	Suppression(%)	N
sma-9(cc604)	1.4±0.2*	1359
tsp-12(jj300); sma-9(cc604)	16.5±0.8	3343
tsp-14(jj95) sma-9(cc604)	1.9±0.3	2347
tsp-12(jj300); tsp-14(jj95) sma-9(cc604)	80.0±1.3	3952
tsp-14(jj368) sma-9(cc604)	20.3±0.3	3078
tsp-12(jj300); tsp-14(jj368) sma-9(cc604)	68.5±2.4	2700

Figure 8